

On the Trail of the Multipotent Adaptor

Protein Fe65:

A Biochemical Approach towards Determining the Binding Affinity and Structure of a Protein Relevant to Alzheimer's Disease.

Diplomarbeit zur Erlangung des akademischen Grades

Diplom-Ingenieurin der Biotechnologie

an der Universität für Bodenkultur

Eingereicht im Februar 2008

von Barbara Nussbaumer

Durchgeführt am Institut für Molekulare Pathologie

in Wien unter der Leitung von Peggy Stolt-Bergner, PhD

“知不知上，不知知病。”

老子

*“To know we do not know is the highest;
Not to know we do know is a disease. ”*

Lao-tse (570 B.C.)

Kurzfassung

Der γ -Sekretase Abbau des Typ-1 Transmembranproteins amyloides Vorläuferprotein (APP) ist bekanntlich die Quelle der cytotoxischen A β -Peptide, welche für die Alzheimer'sche Krankheit mitverantwortlich sind. Bis jetzt ist jedoch wenig bekannt über die intrazelluläre Kommunikation zwischen APP und dem Zellkern in der gesunden Nervenzelle. Fe65 ist vermutlich das Schlüsselprotein dieser Interaktion, weil es der direkte intrazelluläre Adapter des APP Proteins ist. Bekannt ist weiters, dass der APP-Abbau durch Sekretasen die Translokation von Fe65 in den Nukleus auslöst, wo es die Transkription von Zielgenen beeinflusst.

In diesem Projekt lag das Hauptaugenmerk auf der Charakterisierung der C-terminalen Phosphotyrosin Bindungsdomäne (PTB) von Fe65 und ihrer Interaktion mit der intrazellulären Domäne von APP. Es konnte die Dissoziationskonstante dieser Interaktion durch isothermale Titrationskalorimetrie (ITC) bestimmt werden. Außerdem wurden hohe Erträge bei der Aufreinigung der erwähnten stark hydrophoben PTB Domäne, für zukünftige Kristallisationsverfahren, erreicht. Parallel dazu wurde anhand des Modells von Cao et al, 2004, versucht die Frage zu beantworten, ob eine intramolekulare Interaktion von Fe65 stattfindet und dadurch eine höhere Regulierungsebene des Signalweges von APP bildet. Wiederholte Experimente dieser Publikation zeigten nicht die erwarteten Ergebnisse, somit konnte das Modell nicht verifiziert werden. Diese Ergebnisse können uns einen Schritt näher zur Lösung des Rätsels führen, welche physiologische Aufgabe APP in der Zelle erfüllt. In weiterer Folge kann dies natürlich helfen Pannen im System zu finden, welche die Auslöser für die Alzheimer'sche Krankheit darstellen.

Abstract

Degradation of the type-1 transmembrane protein amyloid precursor protein (APP) by γ -secretases is known to be the source of the cytotoxic A β -peptide, which is responsible for Alzheimer's disease. However, only little knowledge was gained so far on the intracellular communication between APP and the nucleus of the healthy nerve cell. Fe65 is thought to be the key protein in this interaction, since it is the direct intracellular adaptor of the APP protein. Upon APP-cleavage Fe65 is known to translocate to the nucleus and regulate gene transcription in complex with other nuclear proteins.

In this project the main focus lay on the characterization of the C-terminal phosphotyrosine binding (PTB) domain of Fe65 and its interaction with the APP intracellular domain. The dissociation constant of this interaction could be determined by isothermal titration calorimetry (ITC). Furthermore improvement of the protein yield of the purification of this strongly hydrophobic PTB domain could be achieved for future crystallization trials. In parallel a second major question was addressed. From a model proposed by Cao et al in 2004, the question whether an intramolecular interaction of Fe65 is taking place and thereby building a higher order of regulation of the APP intracellular signaling was tried to be answered. Some selected experiments of this publication were repeated. However, the results did not verify the model.

Answers to these questions could lead us one step further in unveiling the secrets of the physiological relevance of APP in the cell and the signaling cascade downstream of this important transmembrane protein. In the future this can help to find the malfunctions in this system, which are the triggers of Alzheimer's disease.

Acknowledgements

First of all I want to thank my supervisor Peggy Stolt-Bergner, PhD for being super as a boss in general and w(v)ise by knowing answers to nearly all my questions (and there were a lot of them!). It was not least thanks to her constant support and motivation that I kept my enthusiasm for research and learned how to cope with scientific frustration.

In general I want to thank the IMP for the great atmosphere and the countless wonderful experiences inside and outside the lab. The friends that I found on the first floor I will never forget. Especially the people from the Clausen and Rumpel group I want to thank for being my bench mates, when our group was just started. From scientific discussion in the beginning to all kinds of topics later on, they became great colleagues and friends.

I want to say thanks to all the proof readers of this thesis, for being so patient. All my friends from the study, who went through hard exams and nice courses and parties with me, I am really grateful for these moments in the last five years at Boku. I want to highlight Sandra, Karin, Lukas and Conny my closest friends, who spent days and even nights studying for exams with me.

But without the emotional and financial support from my family the study and the diploma thesis would have been impossible. To define the item family a little bit further, it includes all my three pairs of parents: My dad and his family, my mum and her family and my "Hebenstreit-parents", they all were investing so much energy in me during the past years

Last but not least I want to thank a person that became my enzyme 7 years ago by reducing fear and activating energy before exams and all kinds of hard moments in my life since then. Without him these lines would not be written... thank you for being there Markus!

Contents

KURZFASSUNG	I
ABSTRACT	II
ACKNOWLEDGEMENTS	III
FIGURES AND TABLES	VII
1 INTRODUCTION	1
1.1 Alzheimer's Disease and APP	1
1.2 The Adaptor Protein Fe65	5
1.2.1 Overview: Structure and Function in Development and Disease	5
1.2.2 WW Domain, Binding Partners and Target Genes of Fe65	7
1.2.3 PTB Domains and Binding Partners	9
1.3 Approaches	12
1.3.1 Intramolecular Binding	12
1.3.2 Purification and Characterization of the PTB2 Domain	13

2	MATERIALS AND METHODS	14
2.1	Materials	14
2.1.1	Solutions and Reagents	14
2.1.2	Bacterial Strains and Plasmids	16
2.2	Molecular Cloning Techniques	17
2.2.1	PCR for DNA Amplification and Mutagenesis	17
2.2.2	Agarose Gel Electrophoresis	20
2.2.3	Gel Extraction and Purification	21
2.2.4	Restriction Digest and Ligation	21
2.2.5	Transformation	22
2.2.6	Isolation of Plasmid DNA from Bacterial Cells	23
2.3	Biochemistry	24
2.3.1	Protein Expression and Purification	24
2.3.1.1	Expression Trials	24
2.3.1.2	Large Scale Expression	24
2.3.1.3	Batch Purification of the WW Domain	25
2.3.1.4	Purification of the PTB Domains	26
2.3.2	Protein Analysis	27
2.3.2.1	SDS - PAGE	27
2.3.2.2	Staining	28
2.3.2.3	Western Blot	29
2.3.2.4	Determination of Protein Concentration	30
2.3.2.5	Solubility Screens	31
2.3.2.6	Dynamic Light Scattering (DLS)	33
2.3.2.7	Circular Dichroism Spectroscopy (CD)	34
2.3.3	Binding Assays	36
2.3.3.1	Pull-Down Assay	36
2.3.3.2	Isothermal Titration Calorimetry (ITC)	37

3	RESULTS AND DISCUSSION	39
3.1	Intramolecular Binding	40
3.1.1	Construct Design	40
3.1.2	Purification of Fusion Proteins	43
3.1.2.1	WW-GST Construct	43
3.1.2.2	PTB1+2 full-end MBP Construct	44
3.1.2.3	PTB1+2 MBP Construct	45
3.1.2.4	PTB2 full-end MBP Construct	46
3.1.2.5	PTB2 MBP Construct	47
3.1.3	GST Pull-Downs	48
3.1.4	Synthesis of the WW Domain	52
3.1.5	ITC of the WW Domain	54
3.2	Purification and Characterization of the PTB2 Domain	55
3.2.1	Construct Design	55
3.2.2	Expression Trials	55
3.2.3	Initial Purification of the PTB2 Domain	57
3.2.4	Solubility Screens	58
3.2.5	Optimized Purification	60
3.2.6	Protein Analysis	62
3.2.7	ITC with AICD	65
	CONCLUSION AND FUTURE PERSPECTIVES	68
	BIBLIOGRAPHY	A
	APPENDIX	E

Figures and Tables

Figure 1: Scheme of the healthy brain compared to the AD brain.	1
Figure 2: APP position in the membrane and secretase degradation	4
Figure 3: Predicted domain structure of Fe65	5
Figure 4: 3D structure of the Fe65 WW domain	7
Figure 5: 3D Structure of Fe65L1 PTB2 domain	10
Figure 6: Model of Fe65 activation by APP binding	12
Figure 7: plasmid maps	16
Figure 8: scheme of DLS measurement.	34
Figure 9: schematic diagram of ITC instrument setup.	37
Figure 10: Amino acid sequence of Fe65	41
Figure 11: Constructs for the intramolecular binding approach.	42
Figure 12: SDS-PAGE of GST-WW construct.	43
Figure 13: SDS-PAGE of MBP-PTB1+2 full-end construct.	44
Figure 14: SDS-PAGE of MBP-PTB1+2 construct.	45
Figure 15: SDS-PAGE of MBP-PTB2 full-end construct.	46
Figure 16: SDS-PAGE of MBP-PTB2 construct.	47
Figure 17: Western Blot of GST Pull-Down assay	48
Figure 18: Western blot of GST Pull-Down assay	49
Figure 19: ITC measurement with AICD, PTB2 domain (A) and PTB2-MBP (B)	50
Figure 20: CD spectrum of the WW domain of the human yes associated protein	52
Figure 21: CD spectra of the WW domains	53
Figure 22: ITC measurement of WW domain with Fe65-1 peptide (A) and with Mena peptide (B).	54
Figure 23: Constructs used for the PTB domain characterization	55
Figure 24: SDS-gels of cell screen	56
Figure 25: SDS-Page of Purification steps of PTB2.	57
Figure 26: examples of ThermoFluor data from PTB2 (A) and PTB2-MBP (B)	58
Figure 27: Summary of thermoFluor results	58
Figure 28: Chromatogram-overlay of a superdex-75 size exclusion chromatography of PTB2.	60
Figure 29: Second size exclusion chromatography step for PTB2	61

Figure 30: FPLC-Chromatograms of PTB1+2 of the first (A) and the second (B) size exclusion chromatography steps.	61
Figure 31: DLS measurement of PTB2 (purple) and PTB2-MBP fusion protein (blue).	62
Figure 32: CD spectra of Fe65.	63
Figure 33: CD spectrum of the PTB2 domain.	64
Figure 34: ITC measurement of buffer blank with APP peptide	65
Figure 35: ITC measurement of PTB2 with APP peptide	66
Figure 36: ITC measurement of mutated APP peptide and PTB2 domain.	67
Figure 37: pre-stained (left) and unstained (right) Page Ruler from Fermentas	E
<hr/>	
Table 1: Genotypes of bacterial strains.....	16
Table 2: Components used for PCR reaction.....	18
Table 3: List of Primers.(in red ... restriction sites).....	19
Table 4: Components used for ligation reaction.....	22
Table 5: SDS-gel recipe (15% acrylamide).....	28
Table 6: Pull-Down assay setup and expected results ,.....	48
Table 7: 96 ThermoFlour buffer conditions.....	F

1 Introduction

1.1 Alzheimer's Disease and APP

About 18 million people globally are suffering from Alzheimer's disease (AD). Due to the growing average lifespan this number will increase dramatically in the oncoming years.¹

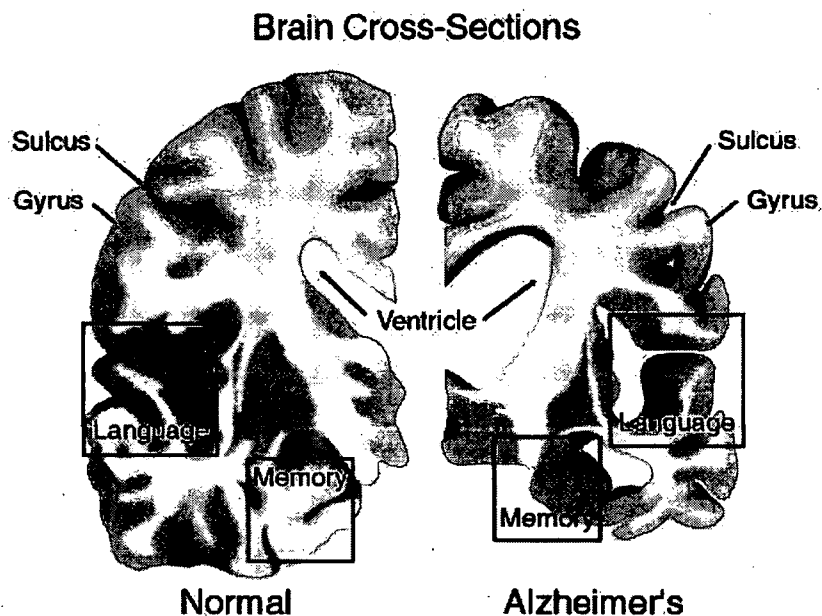


Figure 1: Scheme of the healthy brain compared to the AD brain.²

In this Figure the loss of volume of the brain during Alzheimer's disease as well as the main affected regions in the brain are shown in comparison to the healthy brain.

Alzheimer's disease pathology was first described by Alois Alzheimer in the early 20th century with two main symptoms that could only be attested post mortem: neuritic plaques and secondly neurofibrillary tangles (NFTs). The plaques, built up of A β protein particles, are extracellular (see later in this

¹ World Health Organization, 2000, The World Health Report 2000.

² Adapted from URL: www.crystalinks.com/alzheimers.html [20.11.2007].

section) and the tangles, composed of tau protein released from collapsing microtubules, are within the neurons.

However, diagnosis of AD in elderly people (over 65) is difficult in the early stage, since the normal loss of brain potential due to ageing starts in a similar manner. Patients complain about memory loss as well as the decreasing ability to think, plan and create new memories. Early onset AD starts before the age of 65 and is identified more easily. This kind of AD raises more social problems, since younger patients often still have small children and work. Only in later stages do patients lose the ability to speak, recognize people and orient in a room.³

The actual trigger of the disease is not known until now. There are many different theories. However, it has become clear that a transmembrane protein named the amyloid precursor protein (APP) is playing the leading part in the Alzheimer's play. Its neurotoxic cleavage product, called A β , causes brain degradation by forming amyloid plaques outside the cells, which may block synaptic clefts and thereby cause cell death.⁴

However, there is still not much known about the physiological relevance of this protein in the healthy cell. Tellingly Christina Tang [Journal of Young Investigators, Oct. 2001, Vol. 5, Issue1] expressed the following: "...scientists don't know why our bodies go to the trouble of making this protein while taking the risk of producing a harmful peptide ...".

APP is a type 1 membrane spanning protein with a large extracellular and small intracellular domain.⁵ There is only little knowledge gained so far about the relevance of APP. There is evidence that it plays a role in the development of the brain as well as in memory formation, since it is found in

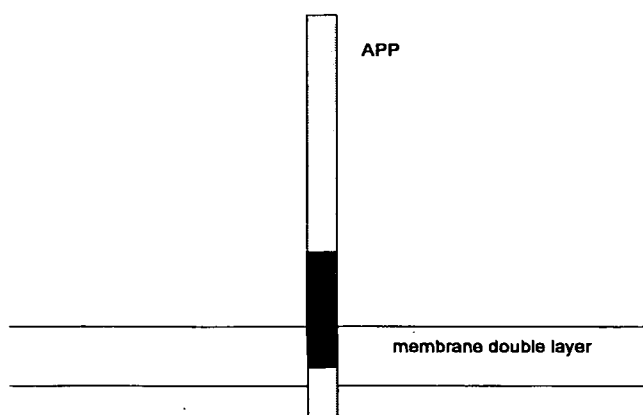
³ Adapted from [URL:http://www.alz.org/alzheimers_disease_what_is_alzheimers.asp](http://www.alz.org/alzheimers_disease_what_is_alzheimers.asp) [07.01.2008]

⁴ Cf. Walsh et al; 2004, Neuron 44: 181-193.

⁵ Cf. McLoughlin DM, 2007, J Neurosci Res, [ahead of print].

vivo in synaptic growth cones and is known to interact with proteins important for neuronal plasticity.⁶ Upon ligand binding to the extracellular domain, APP undergoes regulated intramembrane proteolysis (RIP), whereas the ligands and the function of this proteolysis are still unknown. Figure 2 shows the cleavage of APP by α -, β - and γ -secretase and the resulting products, some of which can be cyto toxic. In the healthy cell γ -secretase produces around 10% of the toxic $A\beta_{42}$ by intramembrane proteolysis. In the Alzheimer's disease brain this increases dramatically.⁷ During about 10 years of suffering up to half of the nerve cells of the human brain die.⁸ The actual role of APP in the healthy cell can only be studied by following its intracellular interaction pathways.

Most Alzheimer's research and treatment are focused on the pathological APP secretase cleavage and ways of reducing the amount of the cyto-toxic $A\beta$ particles in the intercellular lumen. However, the whole process must be initiated by signaling inside the cell, therefore it is important to focus on the intracellular signal transduction in the normal and the malfunctioning neuron.



⁶ Cf. Gralle et al, 2006, J Neurobio, [ahead of print]

⁷ Cf. Kasper DL/Braunwald E/..., 2005, p.2583.

⁸ Cf. Ibid..

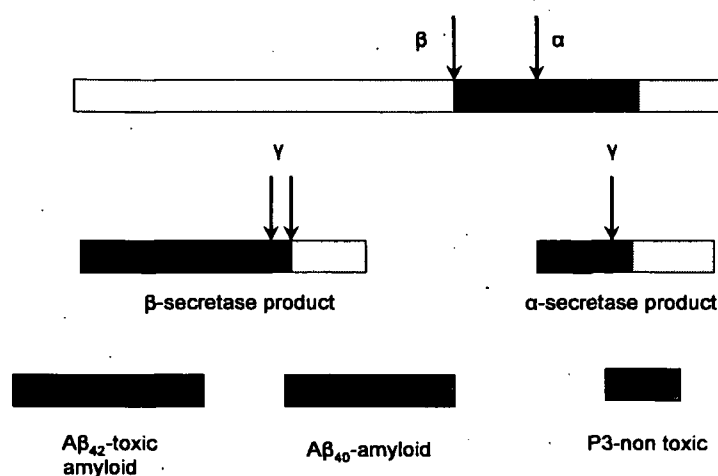


Figure 2: APP position in the membrane and secretase degradation⁹

Figure 2 shows the localization of APP in the membrane as well as the two degradation process ways. The α -secretase cleavage leads to the non-amyloidogenic pathway on the right, whereas the β -secretase cleavage leads to different products of the amyloidogenic pathway, which is shown on the left side of the Figure.

The blue domain in Figure 2 represents the APP intracellular domain (AICD) which interacts with the Fe65 adaptor protein and thereby recruits this protein to the membrane. After γ -secretase cleavage, Fe65 together with the AICD peptide is released. These interactions as well as other Fe65 characteristics have been studied in this project.

⁹ Modified adapted from Kasper DL/Braunwald E/..., 2005, p.2584.

1.2 The Adaptor Protein Fe65

1.2.1 Overview: Structure and Function in Development and Disease

The intracellular APP adaptor protein Fe65 is found in all organisms that possess at least a minimal nervous system. Evidence for this is the existence of a paralogous protein named Feh-1 in *C.elegans*.¹⁰ The family of mammalian Fe65 proteins contains three members: Fe65, Fe65Like1, and Fe65Like2. However, only Fe65 is exclusively expressed in nerve cells.¹¹ The name Fe65 is derived from the initials of the first author and the clone number in a paper describing rat brain cDNA fragments.¹²

It is known from limited proteolysis that Fe65 consists of 3 distinct domains.¹³ From sequence alignments and secondary structure prediction it is assured that these regions are conserved domain structures. After a long unstructured region at the N-terminus the small WW domain spans approximately from amino acid 250 to 290. The WW domain contains two highly conserved tryptophan residues, which give the domain its name. After another long unstructured region the two phosphotyrosine binding domains (PTB) are predicted to follow closely after each other (from aa360-500 and aa540-640).

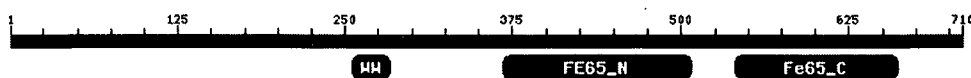


Figure 3: Predicted domain structure of Fe65¹⁴

¹⁰ Cf. McLoughlin DM et al, 2007, *J Neurosci Res*, [ahead of print].

¹¹ Cf. Bressler SL et al, 1996, *Hum Mol Genet*, **5**: 1589-1598.

¹² Cf. Esposito F et al, 1990, *Dev Neurosci*, **12**: 373-381.

¹³ Cf. Lamberti A et al, 2005, *Biosci Biotechnol Biochem.*, **12**: p.2397-2398.

¹⁴ Adapted from URL: www.ncbi.nlm.nih.gov/blast/BLAST/blastp/FormattingResults-MD7UUTFV011 [22.11.2007].

The N-terminal PTB domain (later referred to as PTB1) is binding to different interaction partners at the membrane as well as in the nucleus, whereas the C-terminal PTB domain (PTB2) is thought to bind exclusively to the APP intracellular domain. The WW domain has different interaction partners in the cytoplasm and the nucleus. In the cytoplasm one important interaction partner is a protein called Mena, which is known to play an important role in cell migration and plasticity and therefore in the developing brain and memory formation.¹⁵

Since Fe65 can bind to many binding partners simultaneously via its three domains, it is often denoted as an adaptor protein. However, the fact that makes this protein so interesting is not only its strong binding to the A β producing APP, but also that it is able to translocate to the nucleus, where it may play a role in transcription.¹⁶ It is still unclear if the AICD (APP intracellular domain) is translocated to the nucleus together with Fe65, after APP processing, or not.¹⁷ Fe65 was also shown to affect APP processing, however the results are very contradictory. Especially whether it is enhancing or reducing A β production, when it is bound to APP, is still unclear.¹⁸

Fe65 is activating gene regulatory elements via its WW domain as well as interacting with proteins involved in neuronal migration. This means that understanding the pathways regulated by Fe65 will help us to understand the function of APP in the developing as well as in the AD neuron.

¹⁵ Cf. Sabo L et al, 2003, J Neurosci, 13: p.5407.

¹⁶ Cf. Sabo L et al, 2003, J Neurosci, 13: p.5407.

¹⁷ Cf. McLoughlin DM et al, 2007, J Neurosci Res, p.4 of 11[ahead of print].

¹⁸ Cf. *ibid.*, p.3 of 11.

1.2.2 WW Domain, Binding Partners and Target Genes of Fe65

WW domains are named after the fact that they contain two highly conserved tryptophan (W) residues in their primary structure, which are essential for the structure and function of this domain. WW domains are small protein domains in the size range of about 40 amino acid residues. They consist of three anti-parallel β -strands (see Fig.) and bind to proline rich sequences in other proteins.¹⁹ Like its homologues Fe65L1 and Fe65L2, Fe65 contains one single WW domain N-terminal to the PTB domains. For Fe65, several binding partners were identified: Mena and Evl (members of a family of actin cytoskeleton regulatory proteins), c-Abl tyrosine kinase and some others as described in the following paragraphs.²⁰

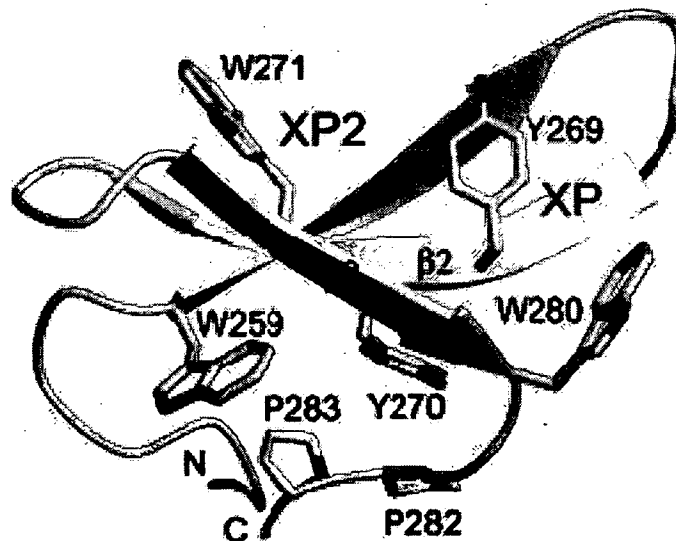


Figure 4: 3D structure of the Fe65 WW domain²¹

In this structure the two conserved tryptophans (W271, W280) are shown in yellow as is the third peptide interacting residue, tyrosine 269.

¹⁹ Cf. Sudol M et al, 2001, FEBS Lett, **490**: p. 190-195.

²⁰ Cf. Ermekova KS et al, 1997; J Biol Chem, **272**: 32869-32877 and Lambrechts A et al, 2000, J Biol Chem, **275**: 36143-36151.

²¹ Adapted from Meiyappan M et al, 2007, J Mol Biol, **372**: 970-980.

Cao et al (2004) proposed a model, in which the WW domain is binding to the PTB domains and thereby impede the binding to other ligands. This inactive state has to be activated by an unknown mechanism in this model. Intramolecular binding therefore can be used by Fe65 to stay in a "resting state" until the WW domain is binding to other ligands with a higher affinity. APP and Fe65 were found to colocalize in neuronal growth cones and focal adhesion points, suggesting potential roles for an APP/Fe65/Mena complex in synaptic plasticity and the developing brain.²² Mena is a regulator of the actin cytoskeleton. The crystal structure of the Fe65 WW domain was solved together with the binding sequence in Mena (Fig. 4), which is a strong binding partner for the WW domain, although the binding is weak (around 120 μ M), when compared to other domain-peptide interactions.²³ Since there are not more than 3 proline residues close together in the region of the PTB2 domain, the binding of the WW domain could be opened by competing ligands easily.

In the nucleus the WW domain of Fe65 plays important roles as well. Most probably the WW domain is also responsible for nuclear translocation of the Fe65/AICD complex, since these proteins do not contain a nuclear localization signal (NLS).²⁴

The nucleosome assembly factor SET has been identified as binding to a region of Fe65 overlapping the WW domain. It is known to assemble together with the Fe65/AICD/Tip60 complex, with Fe65 as a scaffold.²⁵ The following genes were found to be possible targets of this complex: KAI1, thymidilate synthase, GSK3- β , APP, BACE1, neprilysin and Tip60.²⁶

²² Cf. McLoughlin DM et al, 2007, J Neurosci Res, p.6 of 11[*ahead of print*].

²³ Cf. Meiyappan M et al, 2007, J Mol Biol, **372**: 970-980.

²⁴ Cf. Sudol M et al, 2001, FEBS Lett, **490**: p. 190-195.

²⁵ Cf. Telese F et al, 2005, EMBO Rep, **6**: 77-82.

²⁶ Cf. sources in the same order as genes: Baek 2002, Bruni 2002, Kim 2003, von Rotz 2004, Perkington 2004, Pardossi-Piquard 2005 and Chang 2006.

These proteins have in some cases known relevance to Alzheimer's pathogenesis. BACE1 cleaves APP, GSK3- β is a tau kinase²⁷ and neprilysin degrades the A β peptide²⁸. Concluding, Fe65 has a still uncertain and non AICD dependent effect on promoter activity.

1.2.3 PTB Domains and Binding Partners

PTB domains are widely spread among the proteome of the species. However, all proteins containing PTB domains are scaffold or adaptor proteins.²⁹

All PTB domains bind their substrate via formation of an additional anti-parallel β -strand, a process called β -augmentation. The dominating structure of a PTB domain is the β -sandwich. The β -strands form two distinct β -sheets, which lie orthogonal to each other. At the edge of this sandwich the ligand binds to the β 5-strand which forms a basic anchoring pocket and the C-terminal α -helix caps the bound peptide.³⁰

Some PTB domains are binding to phosphorylated tyrosine residues (origin of the nomenclature), however, some do bind to unphosphorylated tyrosines, like the PTB domains of Fe65. The NPXY sequence in ligands is a binding motif for many different PTB domains. The proline, asparagine, and tyrosine are only variable in some rare cases (X stands for any amino acid). Another function that most PTB domains share is the fact that they can bind to phospholipids in the membrane with basic patches in regions distant from their peptide binding groove.³¹

²⁷ Cf. Lovestone S et al, 1994, *Curr Biol*, **4**: 1077-1086.

²⁸ Cf. Vardy ERLC et al, 2005, *Trends Mol Med*, **11**: 464-472.

²⁹ Cf. Uhlik MT et al, 2005, *J Mol Biol*, **345**: p. 1.

³⁰ Cf. Farooq A et al, 2004, *IUBMB Life*, **56**: 547-556

³¹ Cf. see Ref. 29, p 2-3.

With respect to the ligand binding and the differences in structure three classes of PTB domains have been defined:

- ◆ Class 1: IRS-like
 - ◆ Class 2: Shc-like
 - ◆ Class 3: Dab-like
- } Phosphotyrosine dependent Binding

As mentioned earlier the PTB domains of Fe65 are of Dab-like structure and binding mode. Dab-like PTB domains not only do not need phosphotyrosine in the 0 position, but they even disfavor binding to phosphorylated tyrosines. The anchoring pocket is much less basic and binding is not as dependent on the tyrosine in the 0 position. However, a large number of hydrophobic contacts and hydrogen bonds between the peptide and the β 5-strand ensure the binding strength. The amino acids after position 0 on the C-terminus of the ligand are of much higher importance in Dab-like binding compared to Shc -or IRS-like binding, where the end of the ligand turns away from the PTB domain.³²

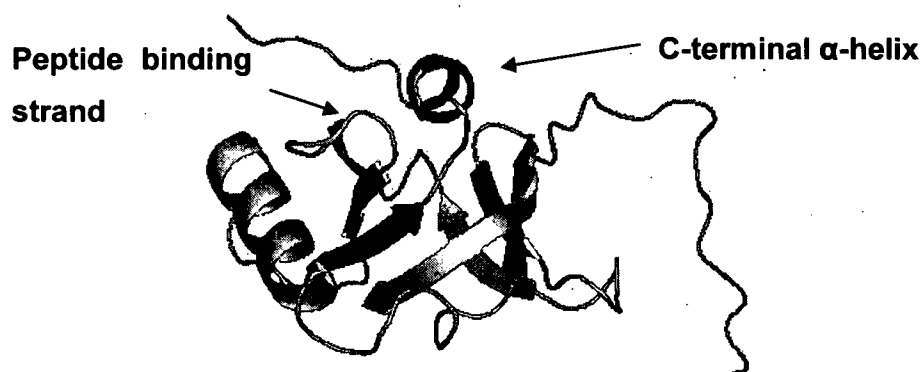


Figure 5: 3D Structure of Fe65L1 PTB2 domain³³

In this 3D structure the β 5-strand for peptide binding and the C-terminal α -helix, which caps the binding groove can be seen.

³² Cf. Uhlik MT et al, 2005, J Mol Biol, 345: p. 5-6.

³³ Source: Protein Data Bank URL:<http://www.rcsb.org/pdb/home/home.do> (search for APBB2) [10.01.2008].

The two PTB domains in Fe65 are of the same class but they differ strikingly in terms of their binding partners. The second PTB domain is binding to one single group of interaction partners, APP and the APP like membrane spanning proteins. This interaction is based on the YENPTY binding motif in the AICD. Binding is regulated by the presence of other APP binding partners and by the possibility of phosphorylation on Thr668 on APP, which impedes Fe65 binding.³⁴

The first PTB domain of Fe65 binds to nuclear proteins and membrane spanning proteins. In the nucleus it binds to the two transcription factors CP2/LSF/LBP1 and Tip60 a histone acetyltransferase.³⁵ The mechanisms regulating the building of this transcriptionally active complex are still unclear.

At the membrane, PTB1 binds to LRP-family receptors and thereby connects APP to other signaling pathways involved in neuronal development. The two LRP family receptors known to bind to PTB1 are ApoER2 and LRP1.

³⁴ Cf. McLoughlin DM et al, 2007, J Neurosci Res, p.4 of 11[*ahead of print*].

³⁵ Cf. Zambrano N et al, 1998, J Biol Chem, **273**: 20128-20133; Cao X et al, 2001, Science, **293**: 115-120 and Kim HS et al, 2003, FASEB J, **17**: U253-U280.

1.3 Approaches

1.3.1 Intramolecular Binding

Figure 4 shows the model that Cao et al proposed, based on their Pull-Down assays using different constructs of Fe65. They were able to show that the WW domain is binding to a sequence between the PTB1 and PTB2 domains. They call the circularized state of Fe65 the "inactive state", and as soon as PTB2 binds to the APP intracellular domain (AICD), Fe65 is proposed to be "activated" and open. Upon APP cleavage it then translocates to the nucleus.

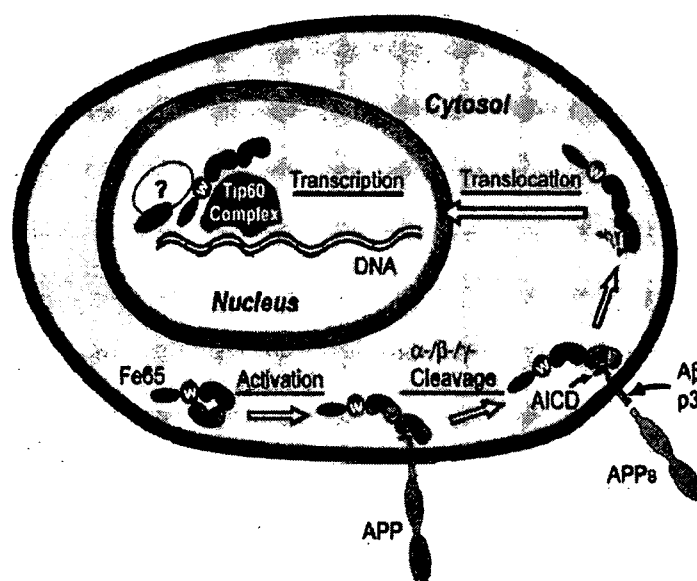


Figure 6: Model of Fe65 activation by APP binding³⁶

Figure 6 shows the intramolecular binding model. First Fe65 has to be activated (released from intramolecular binding) by an unknown process, before binding to the AICD can take place. Upon cleavage Fe65 translocates to the nucleus and transmits a signal.

Is the WW domain really binding intramolecularly and thereby capping the binding sites on the other domains? This question was proposed to be answered in this project by repeating some of Pull-Down assays shown in

³⁶ Modified adapted from Cao X et al, 2004, J Biol Chem 279: 24601-24611.

Cao X et al, 2004. It is known that WW domains bind to proline-rich sequences *in vitro*. In the Fe65 sequence there is no proline-rich motif. There are only two possible regions with more than two proline residues. The first one is just before the beginning of the PTB2 domain and the other one is right after the PTB2 domain. The constructs were then designed containing either one of these regions.

As a second approach, after the Pull-Down assays, ITC measurements were performed to determine the binding strength of the WW domain to peptides of the proline-containing regions in Fe65. Correct folding was checked by circular dichroism spectroscopy. For these ITC experiments the proline rich binding motif from Mena protein functioned as a positive control.

1.3.2 Purification and Characterization of the PTB2 Domain

To find out more about the function and the binding behavior of the domains of Fe65 it would be very helpful to determine the 3D crystal structure of this adaptor protein. The structure of the second PTB domain has been of particular interest in this project. Therefore an individual expression and purification protocol for this domain had to be developed. To characterize the binding mechanism of the PTB2 domain to the AICD in detail ITC measurements were planned. In addition CD measurements should be performed to assure the correct folding of the PTB2 domain after the purification procedure. As a last step, if the purification was sufficient, the PTB domain should be crystallized together with a peptide from the AICD or eventually with the WW domain, if binding is detected.

2 Materials and Methods

In the following section the recipes for the solutions that were prepared by myself and not directly used from the manufacturer are listed separately. Purchased solutions and machines were used after manufacturers' instructions and are mentioned in the respective paragraphs.

2.1 Materials

2.1.1 Solutions and Reagents

From all the reagents used in the described methods the end concentrations of the solutions that were produced by me are listed in the following paragraph. All the purchased articles are not listed here but the source is mentioned in the respective method sections.

Ampicillin: 100mg/mL in 50% Glycerol-H₂O stock, sterile filtered and stored at -20°C.

Ammoniumperoxidsulfat (APS): 10% (w/v) in H₂O, sterile filtered and stored at -20°C.

Chloramphenicol: 35mg/mL powder dissolved in ethanol, stored at -20°C

DNA Lysis Buffer: 50mM Tris HCl, pH 8; 1mM MgCl₂; 1mM EDTA; 1U/mL Benzonase; 200µg/mL Lysozyme.

DTT: powder dissolved to 1M Stock solution in 50% glycerol/dH₂O stored at -20°C

IPTG: powder dissolved to 1M stock solution in H₂O, sterile filtered and stored at -20°C

LB medium: 10 g tryptone, 5 g yeast extract, 10 g NaCl, adjusted to pH 7.0 with NaOH; made up 1 L with ddH₂O and autoclaved. (IMP media kitchen)

Lysozyme: 50 mg/ml in 50% glycerol/dH₂O stock solution, stored at -20 °C.

1 x SDS running buffer: 25 mM Tris/HCl pH 8.3, 200 mM glycine, 0.1% (w/v) SDS.

3 x SDS loading buffer: 0,15M Tris/HCl pH 6.8, 4,5% (w/v) SDS, 15% glycerol, 7,5% mercaptoethanol, 0,15 mg bromophenol blue.

SOB-medium: 20g tryptone, 5g yeast extract, 0,5g NaCl in 1L of deionized water, autoclaved.

SOC-medium: SOB medium plus 20mM glucose.

10 x TAE buffer: 0.4 M Tris/HCl, pH 8.0, 10 mM EDTA-Na₂-salt, 0.2 M acetic acid.

1 x Transfer buffer (TB): 25mM Tris base, 190mM glycine, 10% methanol

1 x TBS buffer: 10mM Tris, 150mM NaCl

1 x TBST buffer: TBS plus 0,05% *Tween 20*[®] detergent

2.1.2 Bacterial Strains and Plasmids

The following *E. coli* strains were used. DH5 α is missing some DNase genes, therefore it was applied for cloning techniques, where a high DNA yield is needed. Rosetta was the strain of choice for expressing foreign (especially eukaryotic) protein, since it carries a plasmid that produces tRNAs mainly used in eukaryotes.

bacterial strain	genotype
DH5 α chemically competent cells	F ⁻ , ϕ 80 Δ lacZ Δ M15 Δ (lacZYA-argF) U 169 deoR recA1 endA1 hsdR17(rk- mk ⁺) <i>phoA supE44 thi-1 gyrA96 relA1</i>
Rosetta TM (DE3) chemically competent cells	F ⁻ <i>ompT hsdS_B (r_B⁻m_B⁻) gal dcm (DE3) pRARE (argU, argW, ileX, glyT, leuW, proL)</i>

Table 1: Genotypes of bacterial strains.

The two plasmids used for protein expression are shown in the following Figure. Purification tags often interfere with biochemical experiments, especially crystallization. The tobacco etch virus protease (TEV) cleavage site after the purification tags makes their removal possible and easy.

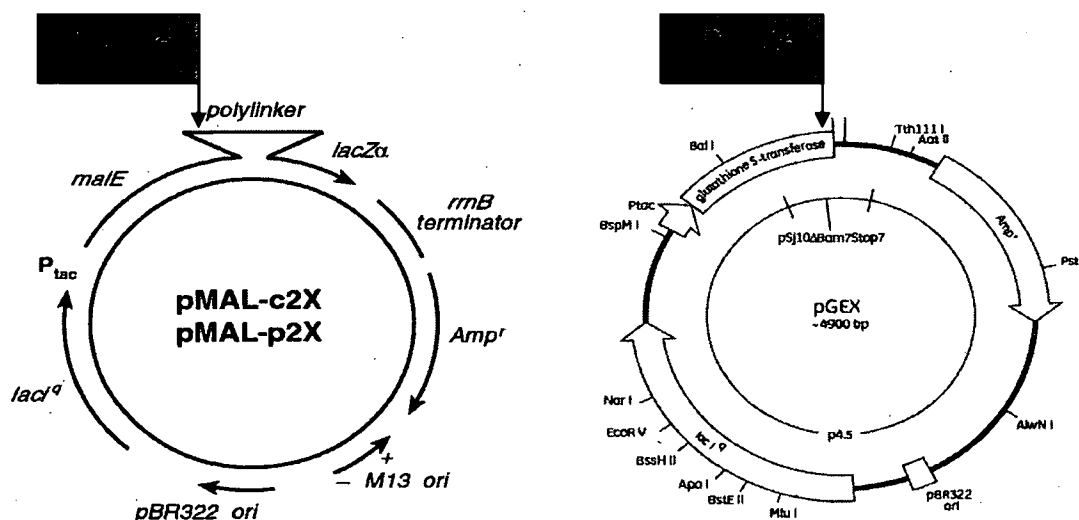


Figure 7: plasmid maps

2.2 Molecular Cloning Techniques

2.2.1 PCR for DNA Amplification and Mutagenesis

The Polymerase Chain Reaction (PCR) is nearly 25 years old, but is still a very efficient procedure for generating large quantities of specific target DNA sequences *in vitro*. However, it is not only used as robust method for amplifying

or isolating DNA but also as a tool for various mutagenesis approaches.

The amplification can be more than a million fold. The essential components (see Table 2) for the reaction are two synthetic oligonucleotide primers (purchased from *Invitrogen*) that are complementary to regions on opposite strands of the target DNA sequence and that, after annealing to the source DNA, have their 3' hydroxyl ends oriented towards each other, in order to enable the DNA polymerase to proceed in the 5' to 3' direction.

In a mutagenesis reaction the deletion, insertion or simple point mutations are built in the primers and amplified by the polymerase. After the normal PCR procedure the template DNA, which is normally from a bacterial source and therefore methylated, can be degraded by DpnI restriction enzyme, which specifically recognizes the methylated DNA. The advantage of the mutagenesis is that the ligation step is not necessary afterwards.

The DNA polymerase is extracted out of thermophilic organisms and therefore can withstand heating to 95° C or higher. Besides the pair of primers also four deoxyribonucleotide triphosphates (dATP, dCTP, dGTP, dTTP) and a suitable buffer (containing magnesium for the enzymatic activity) are necessary for the reaction.

reagent	volume
dNTP-Mix	1 μ L of 10mM stock
Primer 1	2,5 μ L of 10 μ M stock
Primer 2	2,5 μ L of 10 μ M stock
template DNA	approx. 100ng
Buffer	10 μ L of 10x buffer
water dest.	up to 49 μ L
Polymerase	Approx. 1U/50 μ L

Table 2: Components used for PCR reaction

A characteristic PCR process entails a number of cycles for amplifying a specific DNA sequence. Each cycle has three successive steps.

Denaturation: The first step in the PCR amplification is the thermal denaturation of the DNA sample and the primers by raising the temperature to 95° C for at least 15 seconds (for long mutagenesis primers at least 30 seconds). Thereafter the DNA strands are mostly single stranded and can anneal easily to complementary sequences.

Annealing: During the second step, the temperature of the mixture is slowly cooled to ~55° C, this takes about one minute. During this step, the primers base pair with their complementary sequences in the template DNA.

Extension: In the third step, the temperature is raised rapidly to ~72° C, which is optimum for the enzymatic activity of DNA polymerase and is stabilized at that temperature for about one minute. DNA synthesis is initiated at the 3' hydroxyl end of each primer. Then the cycle starts again with the denaturation.

Each step and the temperature changes required during a PCR cycle were carried out in an automated, programmable block heater (Peltier Thermal Cycler PTC-200, MJ Research).

construct and plasmid name	primer pair sequences
PTB2fullend in pMAL	5' CATGCCATGGAAGTGGTGCAGAAG 3' 5' CTAGCTAGCTTATGGGGTCTGAGATCC 3'
PTB2domain in pMAL	5' CATGCCATGGAAGTGGTGCAGAAG 3' 5' CTAGCTAGCTTACTGGGAACGAGCATCC3'
PTB2fullend in pGEX	5' CATGCCATGGAAGTGGTGCAGAAG 3' 5' CGGAATTCTCATGGGGTCTGGG 3'
PTB2domain in pGEX	5' CGGGATCCGAACTGGTGCAGAAG 3' 5' CGGAATTCTCACTGGGAACGAGCATCC 3'
PTB1+2fullend in pMAL	5' CATGCCATGGATCCAGGGATCAAGTG 3' 5' CTAGCTAGCTTATGGGGTCTGAGATCC 3'
PTB1+2domain in pMAL	5' CTAGCTAGCTTAGAGACACTTCTGG 3' 5' CATGCCATGGATCCAGGGATCAAGTG 3'
WW domain in pGEX	5' CGGAATTCTCATGATGGGGAGGCC 3' 5' CGGGATCCACAGATTCCTTCTGG 3'
Quick Change® primers for pMAL mutagenesis	5' gatccgagaacttatacttctaaggcgccatggcta3' 5' tagccatggegccttagaagtataagttctcggatc3'

Table 3: List of Primers.(in red... restriction sites)

The primers were ordered to generate the constructs designed as shown in the chapter Construct Design.

pMAL PCR-mutagenesis was performed to introduce a stop codon after the tag sequence to produce Maltose binding protein as a control for *Pull-Down assays*.

2.2.2 Agarose Gel Electrophoresis

In this electrophoresis method nucleic acid strands are separated according to their molecular weight. The negatively charged phosphate backbones of the nucleic acid (NA) strands are attracted by the anode which is placed on the distal side of the gel. Smaller strands therefore move towards the anode faster. The mesh size (agarose concentration) determines the retention of the moving NA particles and the voltage determines the resolution. Thereby one can quickly determine the yield and purity of a DNA fragment after PCR or restriction digest, etc...

A 1% (w/v) agarose gel was produced, by dissolving the agarose in 1x TAE. The addition of *Sybr*®Safe was necessary for visualization of the DNA fragments. Upon exposure to ultraviolet light, the dye fluoresces with a purple color, intensifying almost 20 fold after binding to DNA. The gel was poured into a casting form provided with a gel comb. 1x TAE functioned also as the electrophoresis buffer. The DNA samples were mixed with DNA loading buffer (*Fermentas*) and placed on the gels in the wells formed by the comb. The electrophoresis was performed for 30 min at 90 V. For gel calibration an adequate DNA size marker (*Gene Ruler, Fermentas*) was additionally loaded on one lane. The DNA intercalating character of *Sybr*®Safe allowed the detection of the DNA fragments under near UV light at 400 nm as separated bands. The intensity of a stained band reflected the amount of DNA in the sample.

2.2.3 Gel Extraction and Purification

DNA gel extraction and PCR purification protocols were performed using the *QIAquick* Gel Extraction Kit (Qiagen) and *QIAquick* PCR Purification Kit (Qiagen) using a microcentrifuge (Eppendorf) according to manufactures instructions. The principle of this purification kit is based on the re-solubilisation of the agarose gel (in case of the gel extraction) and the binding of DNA to silica membranes under high chaotropic salt and low pH conditions. The elution is performed under high pH conditions. The yield of purified DNA is normally in the range of 75% of the applied sample.

2.2.4 Restriction Digest and Ligation

Restriction enzymes are part of the armory of bacteria to defend themselves against foreign (non-methylated) DNA (e.g. Bacteriophages). In molecular biology their property to cleave specific recognition sequences in DNA are utilized to prepare inserts (products from PCR amplification) and vectors of choice for ligation. Therefore the insert and the vector DNA are digested with the same restriction enzymes to obtain matching endings. Enzymes used were purchased from Roche and Fermentas.

The purified PCR products and the vector were digested overnight with standard restriction enzymes or only for one hour with the *Fast Digest Enzymes* (Fermentas) at 37°C. The reaction mix (see Table 4:), contained the suitable buffer system for the respective enzymes. In order to avoid self ligation and to increase the ligation efficiency the digested vector was treated with alkaline phosphatase (AP) during restriction digest. This enzyme removes the 5' phosphates of a cleaved vector.

After the incubation at 37 °C, the restriction digest was stopped by inactivating the enzymes for 10 min at 65 °C. The cleaved vector was analyzed by agarose gel electrophoresis. After the successful digestion of the

vector, the DNA was purified by gel extraction. The inserts were purified by *QIAquick* Gel Extraction Kit to remove the restriction enzymes.

reagents	volumes
Insert	5x molar vector conc. ~3 μ L
vector	150ng ~1 μ L
buffer	2 μ L of 10x buffer stock
T4 Ligase	1U/ μ L
water	up to 20 μ L

Table 4: Components used for ligation reaction

To perform the ligation, insert and dephosphorylated vector were mixed in a 5:1 molar ratio. The reaction mix was incubated with 1 U T4 DNA ligase in the appropriate 10x ligation buffer (containing ATP) at 16 °C-20°C for several hours or at 4°C over night. This enzyme catalyzes the formation of phosphodiester bonds between the vector and the insert. It originates from the T4 bacteriophage and requires ATP as a cofactor.

2.2.5 Transformation

In the transformation step the vector containing the insert is forced by heat shock through the cell membrane into the cytosol of the chemically competent bacterial cell. For the selection of correct clones and later on amplification of the plasmid the vectors were transformed into DH5 α cells, whereas Rosetta (DE3) cells were used thereafter for overexpression of the protein constructs. First the ligation reaction was heated to 65°C for 10 minutes to inactivate the ligase, which can increase transformation efficiency. 100 μ L of cells were transformed with about 150ng of ligation mixture and incubated on ice for 10 minutes before heat shocking at 37 °C for 45 seconds. After chilling the heat shocked cells on ice for some minutes, 500 μ L of SOC

medium were added. The cells could recover while shaking (400rpm) for 30min.

Thereafter the cells were spun down and 500 μ L were taken off and the remaining supernatant was used to resuspend the pellets for plating them out on antibiotic containing LB agar plates. The transformed cells grew over night at 37°C.

2.2.6 Isolation of Plasmid DNA from Bacterial Cells

With the aid of a commercial plasmid preparation kit, named the *QIAprep* Plasmid Mini Kit (Qiagen), plasmid DNA was isolated out of the DH5 α cells. This kit provides all the necessary solutions for cell lysis, chromosomal DNA precipitation and for washing the plasmid DNA bound to a silica column.

Therefore 3-5 ml of LB media containing 100 μ g/mL ampicillin for selection was inoculated with a single bacterial colony of ampicillin- resistant *E. coli* from the selection plates and incubated overnight at 37 °C/ 200rpm shaking. The grown cells were harvested by centrifugation (3500 rpm in Eppendorf centrifuge 5810 R) for 20 minutes and afterwards purified following manufacturer's instructions (Plasmid Mini Kit), according to the alkaline lysis method.

The selection for the cells containing the plasmid was already achieved by growing them on selection plates containing antibiotics.

Now the cells containing the correct plasmid were selected by agarose gel analysis of the restriction digest of small aliquots of the extracted plasmids. Those with the inserts of the right size were then sent to the sequencing department in house (IMP service department), to make sure that actually the right sequence was inserted for further protein production.

2.3 Biochemistry

2.3.1 Protein Expression and Purification

2.3.1.1 Expression Trials

In the following trials cells from over-night cultures were grown in small scale Erlenmeyer shaker flasks with 20mL of LB medium each. The inoculum was 500 μ L per flask.

- Cell screen: This screen was performed to find the best performing E.coli strain (highest expression level). The plasmids containing the PTB2 and PTB1+2 constructs were transformed into different E.coli strains. E.coli strains: BL-21, Rosetta, BL21-pLysS, Rosetta-pLysS. This screen was evaluated by comparison of the recombinant expression levels in the different pre- and post-induction samples on an SDS-gel after 3h of induction.
- Growing conditions: In this screen different induction times and inducer concentrations were tested to find the optimal expression conditions. Isopropyl- β -D-thiogalactopyranosid (IPTG)-concentrations: 0.25mM,0.5mM,0.75mM,1mM; Induction times: 2 hours, 4 hours, over night. This screen was analyzed by interpretation and comparison of the amount of soluble protein of the lysis samples of the different conditions on a SDS-gel.

2.3.1.2 Large Scale Expression

In order to obtain sufficient amounts of protein for the binding assays and solubility screens and further crystallization trials, the constructs of Fe65 were produced in large scale in *Rosetta* cells with either GST or MBP tags for purification.

The transformed cells were first grown in over-night cultures (20-100mL LB medium) in 200mL Erlenmeyer shaker flasks at 37°C and 200rpm. These overnight cultures needed to be grown in the presence of chloramphenicol to stabilize the *pRARE* vector, which is already pre-transformed in the purchased Rosetta cells and ampicillin for the vector of interest. The *pRARE* vector provides the *E. coli* cell with tRNAs that are rarely used in *E. coli* genes, and can be helpful for the expression of eukaryotic genes.

5L shaker flasks were then filled with 2L of LB medium and only ampicillin was added for the selection to reduce stress condition during induction. Between two and six of these 5L bottles (4-12L cells) were used, depending on the amount of protein needed. The induction was performed with 1mM IPTG at OD 0,8 for 18 hours at 18°C and 200rpm. The cells were then centrifuged either in a Sorvall SLC-6000 or a SLC-3000 rotor at about 6000rpm in a cooled Sorvall *Evolution* centrifuge.

2.3.1.3 Batch Purification of the WW Domain

The WW domain was expressed with an amino-terminal GST-tag in front of the construct. The whole purification was performed in the following buffer.

Buffer: 10mM Tris, 150mM NaCl, 1mM EDTA, 1mM DTT.

- **Resuspension:** The cell pellets were resuspended in a sufficient amount of lysis buffer (50mL for 2L of cells)
- **Sonication:** the cells were disrupted 3x for 30 sec. with an ultrasound sonifier and addition of a sufficient amount of lysozyme.
- **Centrifugation:** The lysed cells were then centrifuged in a cooled Sorvall SS-34 rotor for 30min. at 16000rpm
- **Binding to beads:** The supernatant was pored over up to 5mL slurry of glutathione beads (equivalent to 3mL bed volume). This mixture was then incubated for 2hrs at 4°C on a shaker to enable the GST-tagged protein to bind to the glutathione beads sufficiently.

- **Washing steps:** After the incubation time the beads were washed up to five times with the same buffer (10 times bed volume) followed by shaking and spinning down the beads again at maximum 500 x g.
- **Elution:** Elution was performed overnight at 4°C on a rotating plate with 12mL of 10mM glutathione in the buffer. Since the WW-domain was only needed for GST-Pull-Down assays, the protein was left on the beads and no further purification took place.

2.3.1.4 Purification of the PTB Domains

The PTB domains were purified also batch-wise. Only the MBP tagged constructs were purified, because the yield was much higher compared to the GST tagged constructs. The buffer was changed after optimization (see 2.3.2.5) from Buffer 1 to Buffer 2:

Buffer 1: 10mM Tris pH 8, 75mM NaCl, 7% Glycerol, 1mM DTT, 0,5mM EDTA

Buffer2: 20mM Sodium phosphate pH 7, 75mM NaCl, 5% Glycerol, 1mM DTT, 0,5mM EDTA

- **Resuspension:** The cells were resuspended in 50-200mL buffer in the presence of *Complete* protease inhibitor mix from Roche.
- **Disruption:** Three cycles in the French press machine were sufficient for lysis of the cells. However, for frozen cell pellets sonication was used, to avoid damaging the French press with the highly viscous lysates. The sonication was then performed for 5 min in 1 second pulses.
- **Binding to beads:** After centrifugation of the lysed cells the supernatant was incubated with the beads for 2h up to overnight. Max. 10mL beads were used for 6L of cells (8mL bed volume).

- **Wash and Elution:** Max. 3 washes were performed with five bed volumes of buffer, in order not to lose too much protein. Elution was performed on the column with 10mL of 15mM maltose-buffer after pouring the beads into a column.
- **Gelfiltration:** A *superdex-75* (HiLoad 16/60 prep grade) gel filtration column (GE Healthcare) was used for further purification of the eluted fusion protein.
- **TEV-cleavage:** After the cleavage of the MBP tag from the protein construct with the tobacco etch virus (TEV) protease, the TEV protease was removed with the aid of Nickel beads (Ni-Talon resin/ Clontech) binding to the His-tag of the TEV protease and the protein was further purified over a *superdex-75* gel filtration column to remove MBP and newly aggregated protein.

2.3.2 Protein Analysis

2.3.2.1 SDS - PAGE

Reducing Sodium Dodecylsulfate-PAGE (polyacrylamide electrophoresis gel) is a technique used to separate and analyze denatured proteins.³⁷ The anionic detergent SDS binds to the polypeptide chain and confers a negative charge to the polypeptide in proportion to its length, if added in excess. Therefore, the amino acid sequence does not influence the speed or resolution of the moving protein but only its size. Mercaptoethanol in the sample buffer further denatures the proteins by reducing disulfide linkages. Protein samples are sieved by migration through the polyacrylamide gel according to its mesh size (percentage of acrylamide). The stacking and separating gels were prepared as described in Table 5: SDS-gel recipe.

³⁷ Cf.: Laemmli, 1970, Nature, 227, p. 680-685.

Reagent	Resolving Gel	Stacking Gel
sterile water	2,4mL	6mL
Tris 8.8/6.8	2,5mL	2,5mL
SDS	100 μ L	100 μ L
acrylamide	5mL	1,4mL

Table 5: SDS-gel recipe (15% acrylamide)

After mixing all the components in the yellow boxes together APS and Temed were added to polymerize the gel within minutes. The gels were poured into a casting form which allows a simultaneous production of 2-10 mini-gels (approximate dimensions: 80 x 60 x 0,75 mm). Immediately after pouring, the separating gel was overlaid with isopropanol, which was removed after polymerization. The stacking gel was applied on top of the polymerized separating gel after a comb with 15 wells was inserted. Protein samples after cell lysis, during protein purification, from fractions of size-exclusion chromatography as well as *Pull-Down* samples, etc. were mixed in a 1:2 ratio with 3 x SDS loading buffer and heated for 5 min at 95 ° C. After filling about 10 μ L of sample into the wells the proteins were separated at 25mA per gel, until the dye-front ran out of the gel. A molecular weight marker (5 μ l of Fermentas, *PageRuler* Protein Ladder) was loaded on one lane to enable the estimation of the protein sizes. The gels were either stained with *PageBlue*TM solution (2.3.2.2) or used for western blot analysis (2.3.2.3).

2.3.2.2 Staining

Coomassie Brilliant Blue is an aminotriarylmethane dye that forms strong but non covalent bonds with proteins. A combination of van der Waals

forces and electrostatic interactions with the amino-groups keeps the complexes together.³⁸

Coomassie Brilliant Blue R-250 and G-250 dye are used as staining dye for proteins. The latter dye has the lower detection limit of 5ng protein per band and it does not need to be dissolved in methanol or other toxic compounds.³⁹ Staining of SDS gels was performed with the *PageBlue*TM dye from Fermentas, which contains the G-250 dye. The gel was washed first with steaming hot RO water three times for 5 minutes. Then 20mL of the dye likewise steaming hot were added for 20min. To remove the unspecific bound dye the gel was rinsed for 5 min with RO water. All the staining steps were performed on a shaker-plate.

2.3.2.3 Western Blot

Electrophoretically separated proteins are transferred from a gel to a solid support for detection with selective antibodies. Proteins can be identified and quantified roughly with this method.

The SDS-gels for western blotting, such as the gels from the Pull-Down assays, were not stained as described in the previous section. Those gels were placed on a polyvinylidenefluoride (PVDF) transfer-membrane (Millipore) and exposed to an electric field in the environment of 1 X TB buffer in a blotting chamber. The membrane has to be soaked in methanol before use, to make the membrane hydrophilic. In the blotting chamber the proteins on the gel move under voltage from the anode to the cathode direction and thereby into the membrane. Also diffusion and capillary effects cause the movement into the membrane, but to a negligible extent. The membrane was then rinsed with TBST for ~1 minute and after that the

³⁸ Cf. Sambrook J, 2001, Appendix 8.46

³⁹ Adapted from URL: www.fermentas.com/catalog/electrophoresis/proteinstaining.

blocking solution (5% dried milk in TBST) was applied on the membrane to fill the empty surface around the bands with protein to avoid unspecific antibody binding. After an additional washing step with TBST the membrane was incubated over night with the 1:10000 diluted horseradish-peroxidase (HRP) conjugated antibodies (anti-MBP or anti-GST) from New England BioLabs. After another washing procedure (5 x 5min.) with TBST the *Lumigen* developing Kit from Fermentas was applied to the membrane. After 2 min. of incubation with the developing solution the membrane was exposed to a chemiluminescence film (*Hyperfilm*TM, Amersham Biosciences) in a dark room for some seconds up to 5 minutes. The film was further on developed in the dark room.

2.3.2.4 Determination of Protein Concentration

To estimate the protein concentration, the absorption of the purified protein in buffer was measured at 280nm in the spectrophotometer. The buffer alone served as the blank in these measurements. For a more accurate determination of the concentration a wavelength scan from 240-340nm was performed with the spectrophotometer (Ultrospec 3300pro/Amersham Biosciences). The peak at 280nm was then read out as absorption value.

With the aid of the *ProtParam* program⁴⁰ the extinction coefficient could be calculated for any protein sequence that contains tryptophan and tyrosine residues. The concentration was then calculated with the aid of the Lambert-Beer equation:

$$A = \epsilon \cdot c \cdot l$$

Whereas *l* is usually 1 for common cuvettes and therefore the concentration equals the absorption divided by the extinction coefficient. The main drawback of this method is the high contamination sensitivity. One has to take in consideration that any other protein or peptide would be measured,

⁴⁰ URL: www.expasy.ch/tools/protparam.

too. However, it is a fast and simple method to get an accurate concentration value if an extinction coefficient is available.

2.3.2.5 Solubility Screens

- Buffer trial: Cells with the recombinant PTB2 domain were lysed in different Buffer conditions, and the insoluble protein was segregated from the soluble fraction by centrifugation (10min/14000rpm). The amount of soluble protein present in each condition was roughly quantified by SDS-PAGE.

6 different buffers: (10% Glycerol, 1mM EDTA, 5mM DTT in all buffers)

a) 20mM sodium phosphate, 150mM sodium chloride, pH 8

b) 20mM Tris, 150mM sodium chloride, pH 8

c) 20mM sodium phosphate, 300mM sodium chloride, pH 8

d) 20mM Tris, 300mM sodium chloride, pH 8

e) 20mM Tris, 150mM ammonium monosulfate, pH 8

f) 20mM sodium phosphate, 150mM ammonium phosphate, pH 8

- Thermofluor: The principle of this experiment is the fact that hydrophobic patches of proteins are buried in the interior and are inaccessible in the native state. The SYPRO™Orange (Invitrogen) dye is only binding to hydrophobic residues; therefore it attaches only to denatured proteins and starts to fluoresce. In a thermofluorimeter proteins are heated up together with this dye in different buffers to determine the melting temperature, which is correlated with the protein solubility and stability in these buffers. Table of Thermofluor buffers used for this experiment can be found in the Appendix.

- Solubility cleavage screen:

The purified MBP fused PTB2 domain (see 2.3.1.4) was mixed with the following buffers (listed below) in 500 μ L aliquots. The buffers were in 2x concentration and mixed to the protein solution in 500 μ L aliquots. TEV- protease was added for proteolytical cleavage of the MBP tag at 4°C over night. All the buffers were 50mM in the final concentration and 10% glycerol was added. Then the tubes were centrifuged at 14000rpm for 5 min. to segregate the precipitated protein from the solution. The supernatant was mixed with loading buffer and after boiling; the samples were run on a 15% SDS gel to estimate the amount of soluble and cleaved protein. (TEV is only active in reducing environment, therefore 1mM DTT was always present in the cleavage samples.) The APP-Peptide was at least twice as concentrated as the PTB2 domain. Buffers 1-11 are from the commercial Solubility Kit (Jena Bioscience).

1. Potassium phosphate pH 5
2. Potassium phosphate pH 7
3. Hepes pH 7,5
4. Tris pH 7.5
5. EPPS pH 8
6. Imidazole pH 8
7. Bicine pH 8.5
8. Tris pH 8.5
9. CHES pH 9
10. CHES pH 10
11. Tris + APP-peptide pH 8.5
12. 10mMTris/ 150mMNaCl pH 8
13. 10mMTris/ 150mMNaCl pH 8/ APP-Peptide
14. 10mMTris/ 150mMNaCl/ 0.01% TritonX-100 pH 8

- JBS Solubility Kit (Jena Bioscience):

The principle of this test relies mainly on the Dynamic Light Scattering (DLS) analysis of the protein solutions (see next section) to identify a buffer that maintains protein monodispersity. In hanging drops on cover slides the protein was mixed with the test buffer and fixed over a reservoir containing the same buffer. After 24 hours at 18°C the drops were investigated under the microscope and insoluble aggregates in drops were marked and the buffer was not used for further testing. The solubility in the clear drops was checked with the aid of DLS to see if the solutions were monodisperse, which means there are no aggregates. Since there were no monodisperse solutions in the conditions from the first screen, the Additive Screen was applied and the experiment was repeated the same way. In the Additive Screen some common detergents were added to the different buffers.

2.3.2.6 Dynamic Light Scattering (DLS)

Dynamic light scattering (DLS) is a method for measuring average particle sizes in solutions based on the semi-classical light scattering theory. It indicates that light, which impinges on matter, induces polarization of the electrons in the molecules. The factors like frequency shift, angular distribution, polarization and scatter intensity are determined by size, shape and molecular interactions in the sample material.⁴¹ Protein samples after size-exclusion chromatography and after solubility screens were characterized by DLS to determine their particle size and homogeneity.

⁴¹ Cf. Harding SE, Jumel K, 1998, Unit 7.8, p.8-14

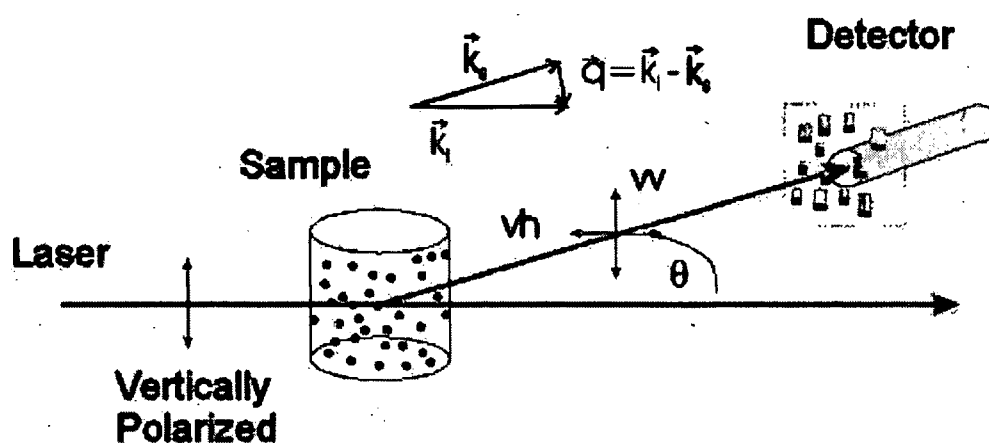


Figure 8: scheme of DLS measurement.

In this Figure the way of the laser ray is shown as red arrow through the sample cell. The amount and the angle of deflected light is collected in the detector.

DLS was performed using a DynaPro-801 molecular sizing instrument (Protein- Solutions Inc.). A 50 μL sample of protein in the purification or screening buffer was centrifuged for 10 minutes at 4 $^{\circ}\text{C}$ /12000 rpm (eppendorf 5415 D) to spin down dust particles and large aggregates of denatured protein, and was transferred into a 45 μL sample cell. The DLS measurements were performed at 19 $^{\circ}\text{C}$. The data were analyzed using the Dynamics V6 software (Protein- Solutions Inc.).

2.3.2.7 Circular Dichroism Spectroscopy (CD)

In a CD measurement plane polarized radiation that is passing through a sample consists of two circularly polarized vectors of equal intensity, one right and one left-handed. A chromophore in the sample would absorb both radiation parts equally and they would be a single plane radiation after the sample again. A CD measurement therefore needs optically asymmetric molecules, which absorb one of the circularly polarized light vectors more strongly or weakly and therefore, when recombined produces an elliptic vector. That difference in absorption is measured as ellipticity. Proteins only give a CD-spectrum because of their tryptophans, tyrosines and phenylalanines in the near UV (240-320nm) and because of the peptide bond in the far UV (180-240nm). These factors are the chromophores of the

proteins and therefore absorb light at a certain wavelength. In structures like the well known α -Helix and β -Strand a certain repetitive conformation of the peptide bond chromophore is produced, which is asymmetric if one considers the whole secondary structure. The ratio of α -Helix and β -Strand in a protein can be determined as well as the folding status, if one has a CD spectrum from the well folded domain to compare to the resulting spectrum.⁴²

To check the folding status of the PTB2 domain after purification as well as synthesized peptides, CD measurement was applied. Samples had to be as pure as possible and were therefore purified over a CD10-desalting column (GE Healthcare). Another important factor to reduce noise signal is the usage of phosphate buffer instead of Tris buffers, since Tris contains a primary amine group per molecule, which causes background absorbance. Far-UV CD spectra were measured in the range from 190 to 260 nm at 1-nm intervals in a cuvette with an optical path length of 10 mm at 20 °C using an Applied Photophysics Pistar-180 spectropolarimeter. After dilution to 1-5 μ M, protein solutions were prepared by centrifugation (5min./10000rpm) immediately before the measurement to prevent any formation of scattering self-assembly products. Buffer base lines were measured under identical conditions and subtracted from the spectra. The data was collected and calculated with the aid of the Π -software. For calculation of the ellipticity and evaluation of the data see results section.

⁴² Cf. Pain R, 2004, Unit 7.6, p 1.

2.3.3 Binding Assays

2.3.3.1 Pull-Down Assay

In a GST-Pull-Down assay a putative interaction of two proteins can be tested in a fast and efficient way. The detection is sensitive and specific, since antibodies are used for identification of the interaction partners.

The GST-tagged WW domain was left on the Glutathione Sepharose™ beads after purification. Then the MBP-tagged PTB2 or PTB1+2 constructs were added in different ratios to the slurry and incubated for about 2 hours at 4°C. The MBP tagged proteins were sometimes added directly in the presence of E.coli lysate to show that non-specific binding is not occurring; however they were mostly used as purified fusion proteins. The disadvantage of the direct method from the lysate is that the concentration of the protein loaded on the beads can only be estimated. After incubation the beads were washed with buffer containing 1% Triton X-100® to remove non-specific binding. Then the samples were mixed with loading buffer and after boiling they were loaded on a 15% SDS-gel. On the western blots of these gels the proteins were detected by antibodies binding to their tags. (Anti-MBP and Anti-GST monoclonal antibody conjugated to horseradish peroxidase)

2.3.3.2 Isothermal Titration Calorimetry (ITC)

ITC is an appropriate method to monitor the interaction of biological macromolecules by measuring the thermodynamic properties of protein-ligand interaction. Aliquots of peptides are injected into a stirred protein sample. As every biochemical reaction is connected to a change in enthalpy (ΔH), either exothermic or endothermic, binding isotherms can be constructed.

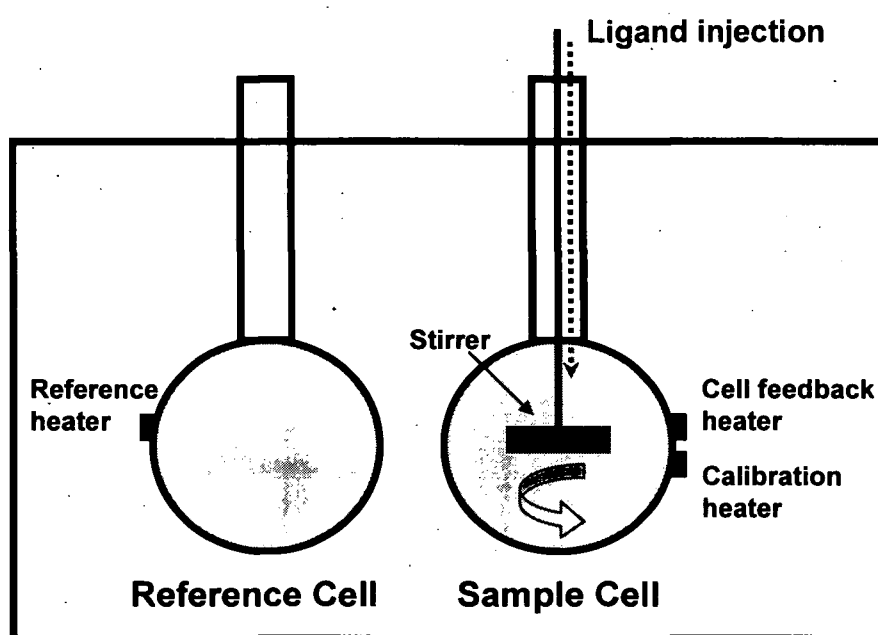


Figure 9: schematic diagram of ITC instrument setup.

Thermophilic detectors time-dependently sense the input of power, which is necessary to maintain equal temperatures in the sample and reference cell, which is filled with water. The enthalpy change associated with binding interactions is determined directly and therefore neither immobilization nor any optical signals are required. For a successful ITC experiment, determination of the initial concentrations of the protein and the ligand is

crucial, since the measured heat change during a calorimetric titration is proportional to the amount of bound peptide.⁴³

ITC experiments were performed on a VP-ITC™ instrument (MicroCal). To reduce non-specific temperature changes, the peptides were dissolved in the same buffer as the respective protein. The sample cell was loaded with 5-10 μM of the PTB2 domain (depending on the output from the purification) whereas the injected APP-peptide concentration was between 7-30 fold of the protein concentration (70-200 μM) in the different runs. The experiments were carried out with 29 injections, each of 10 μl volume, 20 seconds duration and 120 seconds spacing. Analysis of the results and calculation of an approximate k_D value was performed by fixing a single set of binding sites and using the *Origin*™ software.

⁴³ Cf. Pierce et al., 1999.

3 Results and Discussion

Science is facts;

Just as houses are made of stone, so is science made of facts; but a pile of stones is not a house, and a collection of facts is not necessarily science.

Jules Henri Poincaré (1854-1912)

3.1 Intramolecular Binding

3.1.1 Construct Design

The following data, derived from the NCBI - Database⁴⁴, shows the loci of Fe65 in human on chromosome 11 and in rat on chromosome 1, and their official name and source.

```
LOCUS      NP_001155      710 aa      linear      PRI 03-SEP-2007
DEFINITION amyloid beta A4 precursor protein-binding, family B, member 1 isoform E9 [Homo sapiens].
ACCESSION  NP_001155
VERSION    NP_001155.1  GI:4502131
DBSOURCE   REFSEQ: accession NM_001164.2
SOURCE     ██████████ (human)
```

```
LOCUS      NP_536726      711 aa      linear      ROD 25-SEP-2007
DEFINITION amyloid beta (A4) precursor protein-binding, family B, member 1 [Rattus norvegicus].
ACCESSION  NP_536726
VERSION    NP_536726.1  GI:17978453
DBSOURCE   REFSEQ: accession NM_080478.1
SOURCE     ██████████ (Norway rat)
```

The protein sequences are 92% identical, whereas the DNA sequence identity is 88%.⁴⁵ For the experiments in this project the cDNA derived from rat was used.

For the PTB2 domain and the WW domain, solved crystal structures of a homologue and the domain itself respectively helped to determine the domain borders in the amino acid sequence precisely. However, for the PTB1 domain only the secondary structure prediction was available. Several free software programs for secondary structure prediction are available at

⁴⁴ URL: www.ncbi.nlm.nih.gov/entrez/viewer.fcgi?db=protein&id=4502131 [22.11.2007].

⁴⁵ Protein and DNA sequences aligned with the aid of the following free software:

URL: <http://www.ebi.ac.uk/Tools/clustalw2/index.html> [15.11.2007].

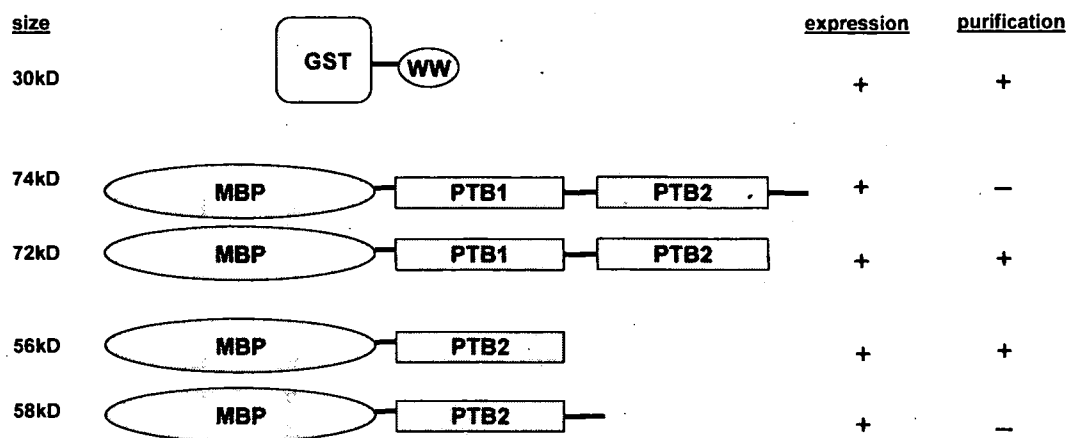


Figure 11: Constructs for the intramolecular binding approach.

All the constructs shown in Figure 11 were cloned successfully into the respective vectors. However, during expression and purification the constructs with the unstructured region after the PTB2 domain showed signs of degradation. These so-called “full-end” constructs seemed to be degraded by proteases either during expression or during lysis. In the following chapter the purification of these constructs is documented.

3.1.2 Purification of Fusion Proteins

3.1.2.1 WW-GST Construct

After affinity purification with glutathione sepharose beads the WW domain fused to a GST tag was purified with the aid of a superdex 200 column (total volume 120mL). The chromatogram of this gel filtration showed one peak at the void volume of the column (40mL) and one soluble WW-GST peak at 87mL. Samples of the fractions were analyzed with SDS-PAGE, which is shown in Figure 12.

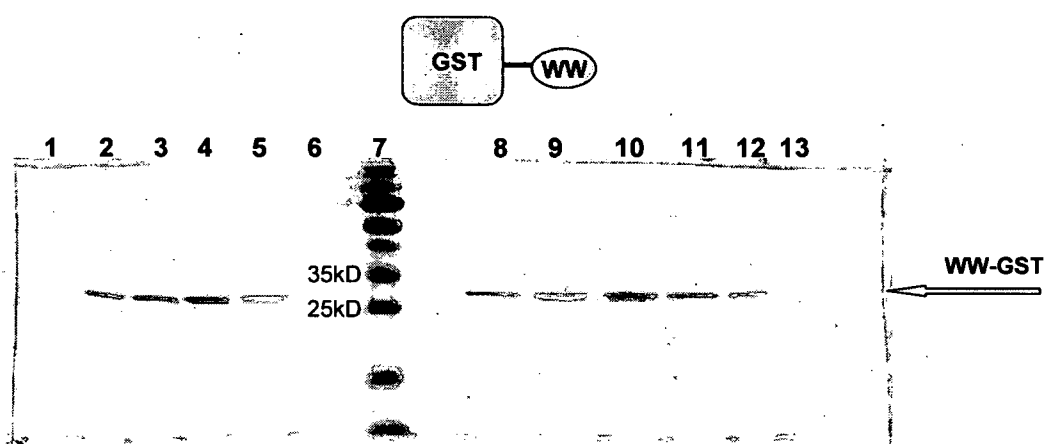


Figure 12: SDS-PAGE of GST-WW construct.

15% SDS-PAGE of fractions containing GST-WW separated on a gel filtration column, 7 μ L of each fraction were loaded.

1-6...fraction of peak at void volume 40mL

7...pre-stained protein ladder (see appendix)

8-13...fractions of peak at 87mL

On the gel it is clear to see that the WW domain, which is 30kD of size, is highly pure. There is about the same amount of protein in the aggregation peak at the void volume as in the soluble peak at 87mL. Much protein is lost due to aggregation, but there is still enough soluble protein from fraction 8-13 for the Pull-Down assays.

3.1.2.2 PTB1+2 full-end MBP Construct

The PTB1+2 construct was purified first by affinity purification and then by size exclusion chromatography with a Superdex 200 column (120mL total volume). The chromatogram of this Gelfiltration showed one peak at the void volume of the column (40mL), two overlapping peaks starting from about 70mL and one final peak at 85mL. Samples of these peaks are shown in Fig. 13.

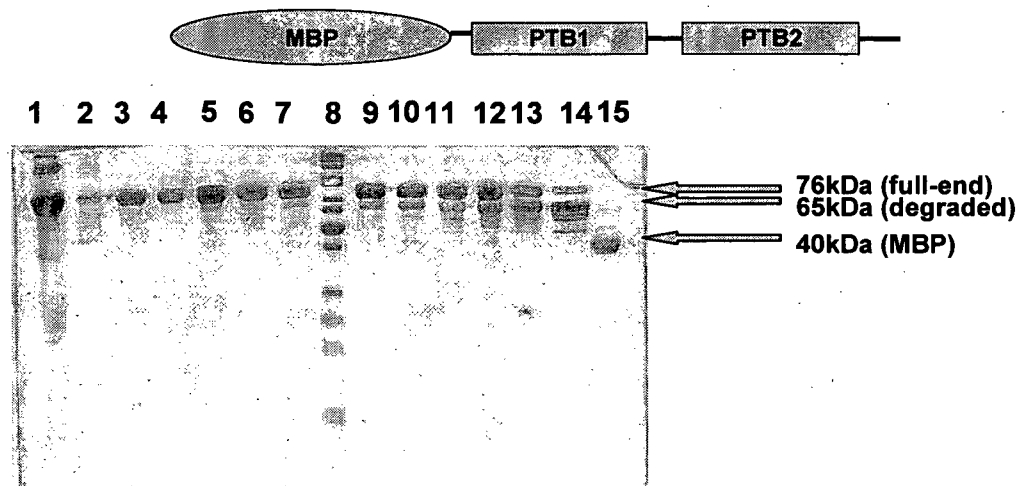


Figure 13: SDS-PAGE of MBP-PTB1+2 full-end construct.

15% SDS-PAGE of fractions containing MBP-PTB1+2 full-end separated on a gel filtration column, 7 μ L of each fraction were loaded.

1, 2... void volume (40mL) of gel filtration column; 3-7... first peak at 75mL

8...unstained protein ladder (see appendix); 9-11... first peak at 75mL

12-14...second peak at 78mL

15...third and last peak on the chromatogram at 85mL

The broad band in the void volume sample implies a large amount of aggregation, which may be due to the high hydrophobicity of the construct. The full-length construct (76kDa) peak overlaps with the peak of the degraded construct (50-65kDa), which can be followed easily over the fraction samples from row 3-14. The degraded construct runs at the same molecular weight (MW), which suggests that the unstructured end is proteolytically digested. The third peak is most likely free MBP from degradation.

3.1.2.3 PTB1+2 MBP Construct

The PTB 1+2 construct was purified with affinity purification and gel filtration with a superdex 200 with 120mL total volume. In the chromatogram a big aggregation peak in the void volume was detected and three peaks of soluble protein at 68-86mL could be seen. In Figure 14 samples of these peaks and the previous purification steps are shown after SDS-PAGE analysis.

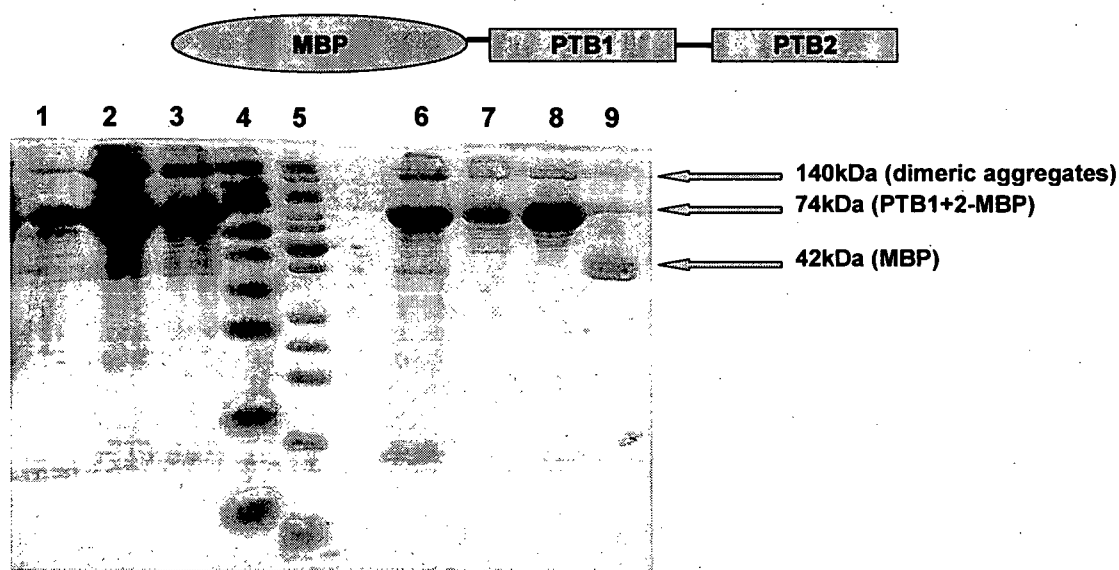


Figure 14: SDS-PAGE of MBP-PTB1+2 construct.

15% SDS-PAGE of fractions containing MBP-PTB1+2 separated on a gel filtration column and of samples from affinity purification, 7 μ L of each fraction/sample were loaded.

- 1...last wash step on the beads; 2...Elution; 3...Beads sample after Elution
- 4...pre-stained protein ladder (see appendix)
- 5...unstained protein ladder (see appendix)
- 6...first peak at void volume 42mL; 7...second peak at 68mL
- 8...third peak at 77mL; 9...last peak at 86mL.

The comparison of lanes 2 and 3 demonstrates nicely, how much protein is lost in the elution step because it is left on the beads. However, this purification gave a high yield of protein as can be seen on the intense bands even after size exclusion chromatography, which dilutes the protein solution by 1.5. Compared to the full-end construct the degradation is insignificant and the protein yield is much higher.

3.1.2.4 PTB2 full-end MBP Construct

In Figure 15 the whole purification procedure of the PTB2 domain construct with end sequence is documented from the expression over the lysis and affinity purification to the last step, the size exclusion chromatography with a superdex 200 column (120mL total volume). Samples from all the 3 peaks of the Gelfiltration and of the previous purification steps are shown after SDS-PAGE analysis.

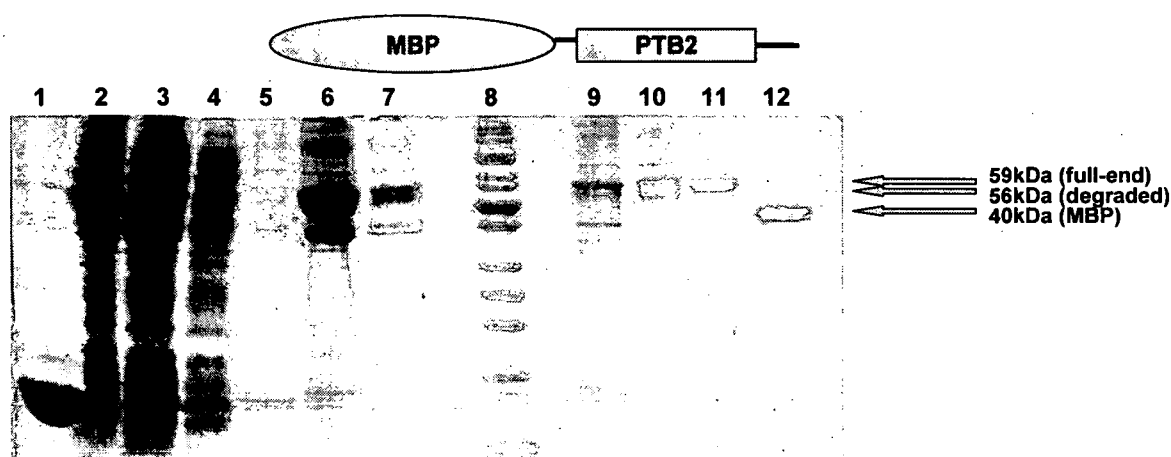


Figure 15: SDS-PAGE of MBP-PTB2 full-end construct.

15% SDS-PAGE of fractions containing MBP-PTB2 full-end, separated on a gel filtration column and of samples from affinity purification, 7 μ L of each fraction/sample were loaded.

- 1...pre-induction sample; 2...post-induction sample; 3...lysis sample
- 4...first wash step on the beads; 5...third wash step on the beads
- 6...elution; 7...beads sample; 8...unstained protein ladder (see appendix)
- 9,10...fraction from peak at void volume of column (45mL)
- 11...fraction from peak at 80mL; 12...fraction from peak at 88mL

In Figure 15 the high purity after the gel filtration is conspicuous. Again the end sequence seems to become degraded, since a second band is seen underneath the band representing the construct at 58kDa. However, in contrast to the PTB1+2 full-end construct the majority of the degraded construct can be found in the void volume peak. As in the other purifications some MBP comes off as a last peak from the size exclusion chromatography.

3.1.2.5 PTB2 MBP Construct

In Figure 16 the whole purification procedure of the PTB2 domain construct is documented from the expression over the lysis and affinity purification to the last step, the size exclusion chromatography with a superdex 200 column (24mL total volume). Samples from all the 3 peaks of the gel filtration and of the previous purification steps are shown after SDS-PAGE analysis.

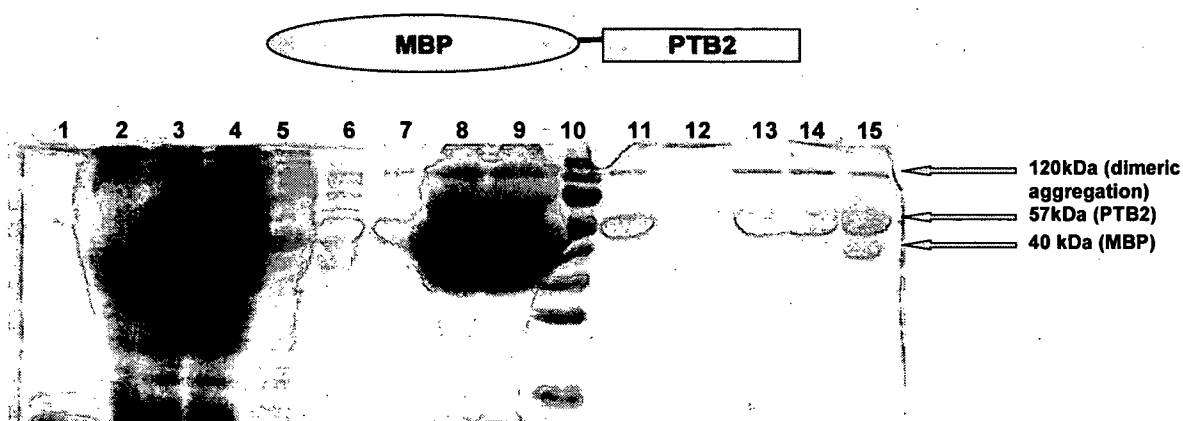


Figure 16: SDS-PAGE of MBP-PTB2 construct.

15% SDS-PAGE of fractions containing MBP-PTB2, separated on a gel filtration column and of samples from affinity purification, 7 μ L of each fraction/sample were loaded.

- 1...pre-induction ; 2...post-induction; 3... lysis sample
- 4...flow through from the beads; 5-7...three wash steps; 8...elution
- 9...beads sample; 10...pre-stained protein ladder (see appendix)
- 11-13...fraction of peak at void volume at 10mL
- 14...fraction of peak at 15mL; 15...fraction of peak at 16mL

Figure 16 shows the well established purification protocol of the PTB2 domain, with high protein yields, but also many losses during elution and due to aggregation in the size exclusion chromatography.

3.1.3 GST Pull-Downs

Table 6 shows the expected results for the Pull-Down assays. There should be hardly any binding detectable for PTB2 in contrast to the strong binding that was shown previously for PTB1+2.⁴⁷ As controls, MBP was loaded on to the WW containing Glutathione-sepharose beads as well as on beads containing just the fusion tag GST. Both were used to exclude non-specific binding.

Input/Pull-Down	GST-WW	GST	empty beads
PTB1+2-MBP			
PTB2-MBP			
MBP			

Table 6: Pull-Down assay setup and expected results ,

Red =no binding

Green = binding

Yellow =weak binding

The following results are a representative excerpt of five performed Pull-Down assays with mainly similar results.

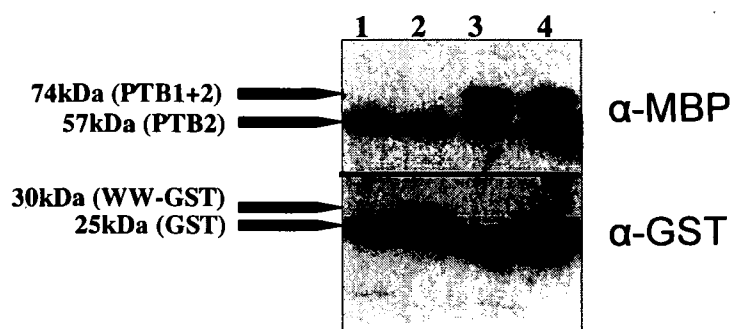


Figure 17: Western Blot of GST Pull-Down assay

Proteins were detected with anti-GST and MBP antibodies (separated for detection).

1... GST + PTB2 MBP (58 kD)

3... GST + PTB1+2 MBP (78 kD)

2... GSTWW + PTB2 MBP (58 kD)

4... GSTWW + PTB1+2 MBP (78 kD)

⁴⁷ Cf.: Cao X et al, 2004, J Biol Chem 279: 24601-24611.

In Figure 17 one can see the same binding in all of the lanes. This means that the Input proteins are binding unspecific to the WW domain. Most probably the background signal from long exposure is so high due to the weak binding that even nonspecific binding to GST can be seen. Furthermore binding of the MBP to the WW domain is detected (data not shown).

In the Pull-Down assay in figure 18 the emphasis lay on the search for the right concentration of the insert protein to find the limiting concentration for the putative binding.

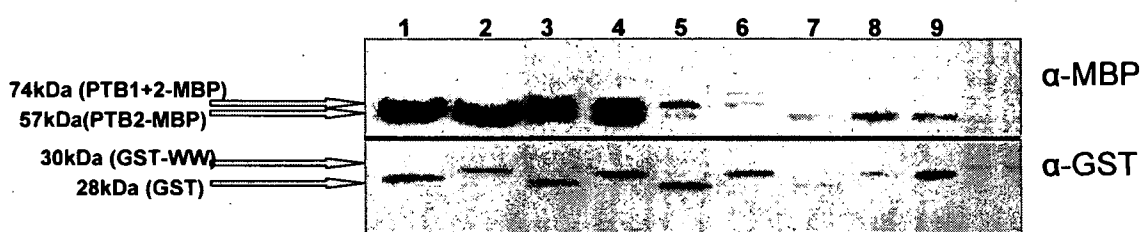


Figure 18: Western blot of GST Pull-Down assay

Proteins were detected with anti-GST and MBP antibodies (separated for detection).

- | | | |
|---------------------|---|--------|
| 1...1μM on GST | } | PTB1+2 |
| 2...1μM on WW-GST | | |
| 3...100nM on GST | | |
| 4...100nM on WW-GST | | |
| 5...50nM on GST | | |
| 6...50nM on WW-GST | | |
| 7...500nM on GST | } | PTB2 |
| 8...500nM on WW-GST | | |
| 9...250nM on GST | | |

However, also in Figure 18 we see no specific binding between the WW domain and the PTB domains. The bands are always about the same intensity with the GST on the beads as with the WW domain on the beads. The blot only shows some unspecific binding that is still detected due to the low detection limit of the western blot.

From the GST Pull-Downs assays one can conclude that there is either no binding between the WW domain and the PTB domains occurring at all and the detected signal is just background, or that the Input proteins are sticking

unselectively to all of the Pull-Down proteins because of their unfolded structure.

To test the quality of the Input constructs of the GST Pull-Downs and the influence of the fusion tags in these constructs, ITC measurements were performed. In Figure 19 the results from the ITC measurement of the PTB2 domain, either with the MBP fusion tag or without, together with the AICD peptide are shown.

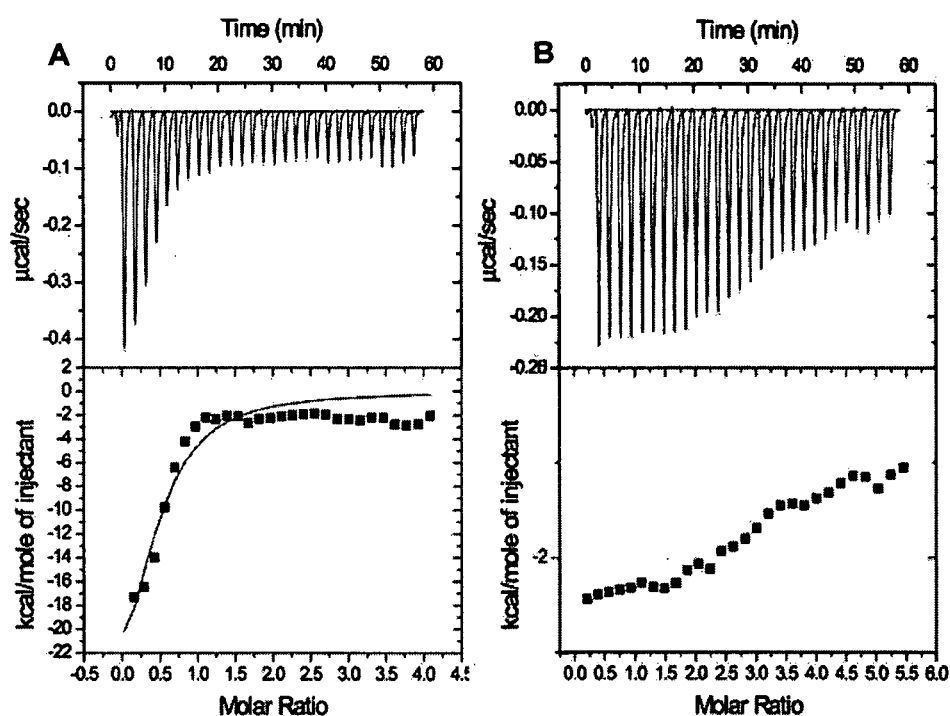


Figure 19: ITC measurement with AICD, PTB2 domain (A) and PTB2-MBP (B)

A: 4 μM PTB2 domain binding to 25 μM AICD peptide, ratio PTB2:AICD = 1:7.

B: 15 μM PTB2-MBP fusion protein binding to 300 μM AICD, ratio PTB2-MBP:AICD = 1:20.

Figure 19 shows that in contrast to the MBP fusion protein the protein domain alone shows strong binding to the peptide. Due to the low binding affinity the dissociation constant for the fusion protein could not be determined.

An explanation for the impaired binding abilities of PTB2 to the AICD peptide when bound to the MBP tag could be that the tag is much larger than the protein. The tag is 40kD in size compared to the PTB2 domain of 14kD. The large tag can be interfering with or simply blocking the binding site. The failure of the GST Pull-Downs can now be explained with the inability of the PTB domains to bind to a ligand as long as the fusion protein MBP is still attached.

3.1.4 Synthesis of the WW Domain

In the last section the GST Pull-Down assays showed unspecific binding of the input proteins to GST, WW-GST, and even to the sepharose beads. Another method to detect binding of two proteins to each other is ITC. Therefore the WW domain was cleaved from the GST tag and the peptides of proline containing sequences of the Fe65 sequence were synthesized (IMP protein chemistry facility). The WW domain was not stable without the purification tag and showed signs of precipitation soon after cleavage. This led to the decision to synthesize the WW domain, since the main part of the domain is only 20 amino acids long. After synthesis the WW domain was checked for proper folding by CD spectroscopy (Figure 21). Fig 20 shows the CD spectrum of a WW domain of the human yes associated protein in denatured and native state.

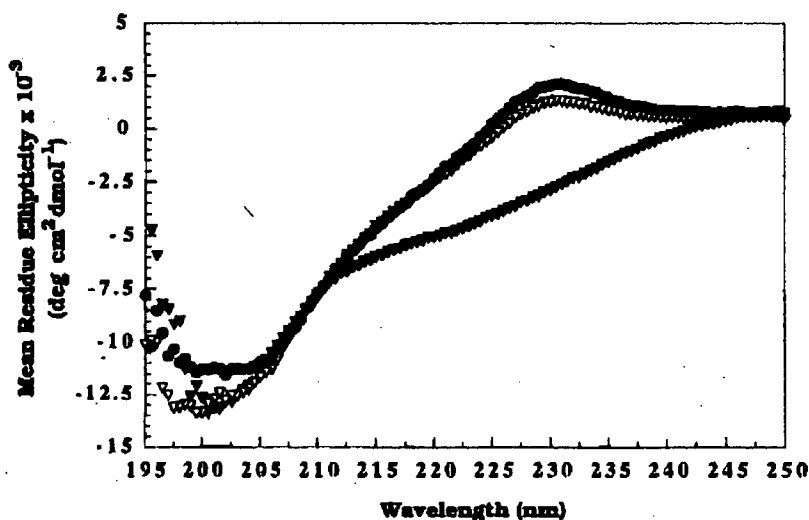


Figure 20: CD spectrum of the WW domain of the human yes associated protein⁴⁸

Spectrum used as comparison to Figure 21. Dotted line...WW domain in 4°C, arrow shaped black line...WW domain in 88°C, arrow shaped white line...WW domain from 88°C after 5min. at 4°C.

⁴⁸ Adapted from Koepf et al; 1999; Protein Sci 8: 841-853.

By comparison of Fig. 20 and Fig. 21 the folding state of the synthesized peptide can be concluded.

Sequences of the synthesized WW peptides:

WW: AGWMRVQDTSGTYYWHIPTGTTQWEPP

mWW: AGWMRVQDTSGTAAAHIPIPTGTTQWEPP

With the following equation the ellipticity was calculated from the raw data:

$$\Theta = (\text{mdeg} \times 100) / N \times l \times c$$

(N= number of amino acid residues; l= path length [cm]; c= concentration [mM])

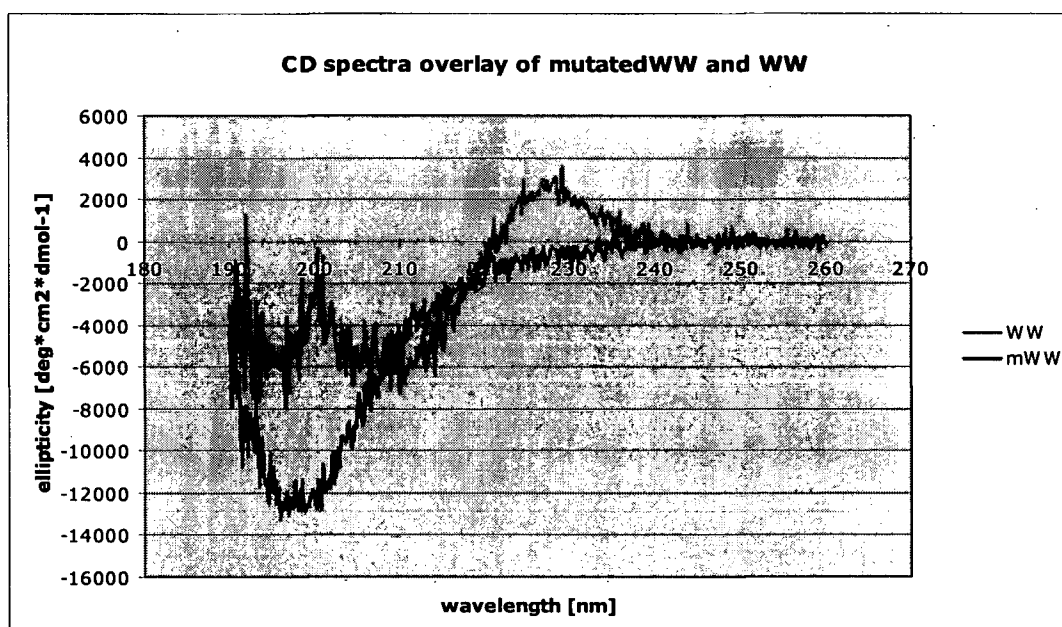


Figure 21: CD spectra of the WW domains

3 μ M WW domain was measured at 20°C in 20mM sodium phosphate buffer.
Red... mWW, Blue... WW

Compared with figure 20 the spectrum of the synthetic Fe65 WW domain (blue) shows the typical 220nm peak from the tryptophan residue. The mutated WW domain (red) without this residue shows a spectrum without this peak. The peak at 200nm represents the folding of the β -sheets. From this spectrum the synthesized WW domains looked well-folded and were therefore further on used for ITC measurements with peptides of the PTB domains.

3.1.5 ITC of the WW Domain

The following peptides were used for this ITC experiment:

Fe65-1: LSLDHSKLVDPVFQVEFPAPKN (In between the PTB domains)

Fe65-1m: LSLDHSKLVDAFQVEFAAAKN (In between the PTB domains mutated → no prolines)

Fe65-2: TSTSLPAPPAESVAR (End of Fe65)

Fe65-2: TSTSLAAAAAESVAR (End of Fe65 mutated)

Mena: PPPPPPPPL (WW binding motif in Mena protein)

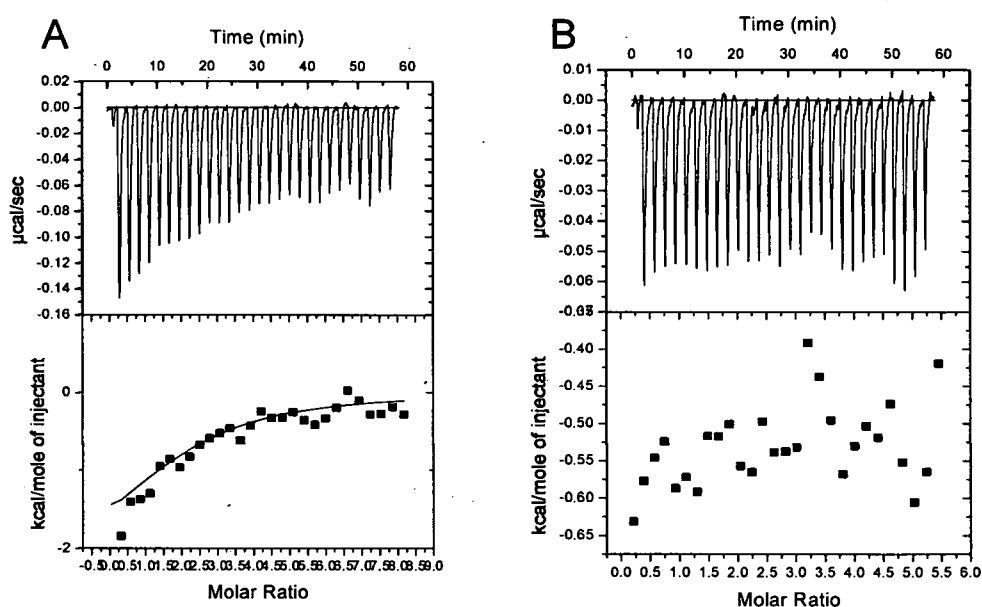


Figure 22: ITC measurement of WW domain with Fe65-1 peptide (A) and with Mena peptide (B).

A: 5 μ M WW domain with 100 μ M Fe65-1 peptide, ratio WW: Fe65-1 = 1:20.

B: 10 μ M WW domain binding to 100 μ M Mena peptide, ratio WW: Mena = 1:10; 10 μ L per injection.

The Mena peptide showed weak binding (about 200 μ M = K_d), but none of the proline-containing motifs of Fe65 showed any binding (data not shown for Fe65-2 peptide). This can also be due to a very weak binding affinity (more than 1 mM K_d) to these targets and therefore binding may be undetectable by ITC. The binding to the Mena peptide seems similar to the published K_d value, but this measurement needs to be repeated.

3.2 Purification and Characterization of the PTB2 Domain

3.2.1 Construct Design

The construct design was identical to the procedure for the “intramolecular binding” approach. The following constructs were used for domain characterization.

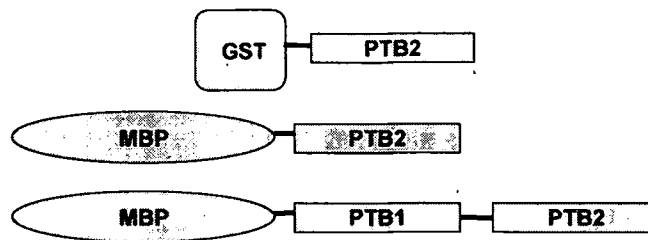


Figure 23: Constructs used for the PTB domain characterization

3.2.2 Expression Trials

Cell screen:

The cells were grown as described in the methods section. After 3h of induction at 18°C in the shaker the post induction sample was drawn. For this cell screen two different GST-PTB2 constructs were tested, to look for the highest expressing cell line. These were constructs during the construct design optimization phase. They were both insignificantly shorter than the end result from construct design. (construct 1...12kD; construct2...10kD).

As can be seen clearly in Figure 24 the highest amount of protein for all the three constructs (see construct design) was obtained from the E. coli strain “Rosetta” (data only shown for GST-PTB2).

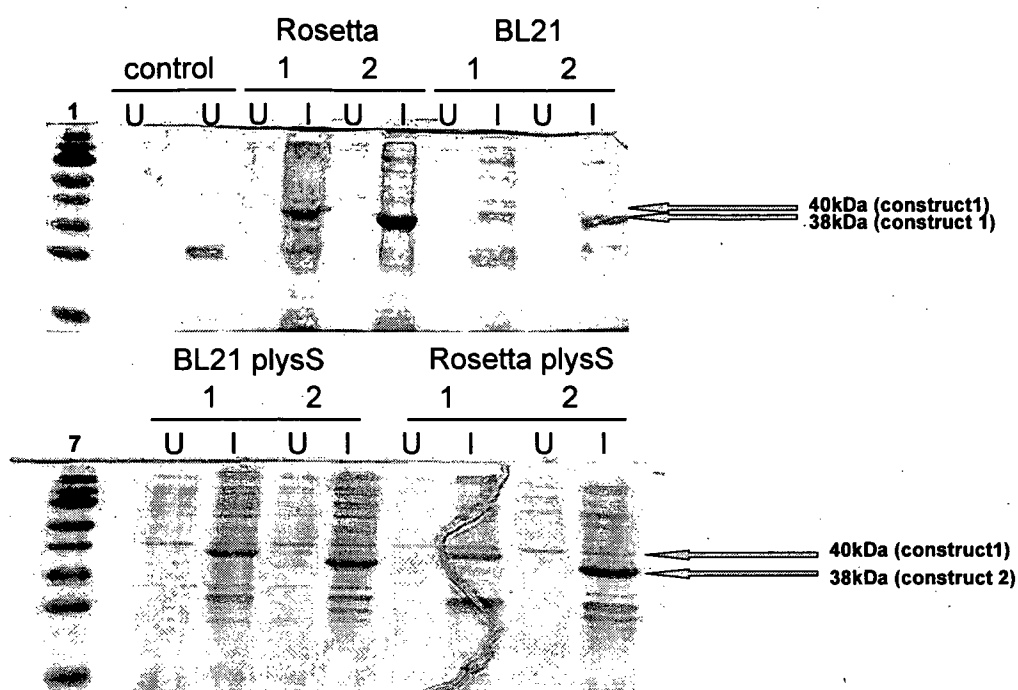


Figure 24: SDS-gels of cell screen

1, 7...pre-stained protein ladder (see Appendix); U...uninduced; I...induced;

Growing conditions:

Rosetta cells were grown under different conditions as described in the methods. From the tested growing conditions the inducer (IPTG) concentration of 0.75 and 1mM gave about the same results (data not shown). The highest recombinant protein concentrations were found in the over night induction at 18°C (about 18hrs.). 1mM IPTG and 18hrs of induction were then used for all the small and large scale expressions.

From the cell screens the cell line and the expression conditions could be determined in which the highest recombinant protein yield was obtained.

3.2.3 Initial Purification of the PTB2 Domain

The PTB2 domain is a strongly hydrophobic protein domain. It contains only 19 charged amino acid residues in its 150 amino acids. Therefore purification is difficult and much protein is lost due to aggregation. Figure 25 shows that in the initial purifications the protein yield was not very high and the protein was unstable in the Tris (pH 8) buffer. Therefore further buffer screens were performed.

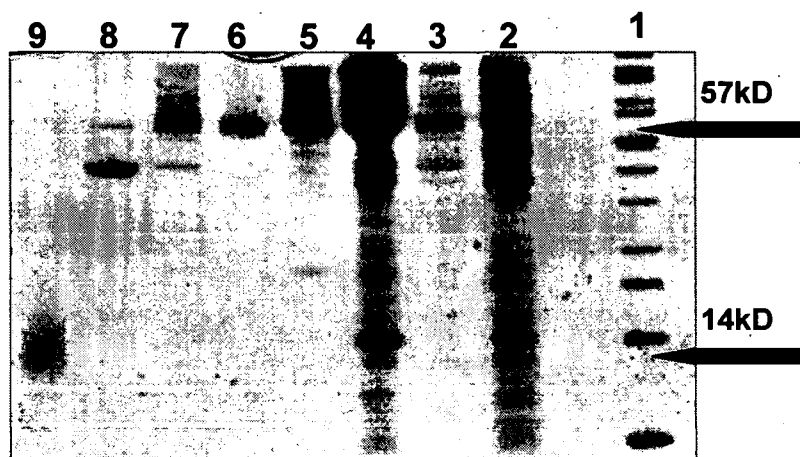


Figure 25: SDS-Page of Purification steps of PTB2.

15% SDS-PAGE of fractions containing MBP-PTB2, separated on a gel filtration column and of samples from affinity purification, 10 μ L of each fraction/sample were loaded.

- 1...unstained protein ladder (see appendix)
- 2...Flow through from affinity beads.
- 3...last washing step of affinity column.
- 4...Elution of MBP fusion protein.
- 5...aggregation peak on first size excl. column.
- 6...PTB2 soluble peak (green in Figure 28).
- 7...between soluble peak and MBP peak
- 8...MBP peak. (yellow in Figure 28)
- 9...PTB2 on second size excl. column after TEV cleavage

3.2.4 Solubility Screens

As described in the Methods the following buffer screens were carried out: Buffer trial, Thermofluor, solubility cleavage screen and JBS solubility Kit.

Buffer trial:

In the buffer trial, the sample with sodium phosphate buffer at pH 8 showed the highest yield of eluted protein in this small scale purification experiment (data not shown).

Thermofluor:

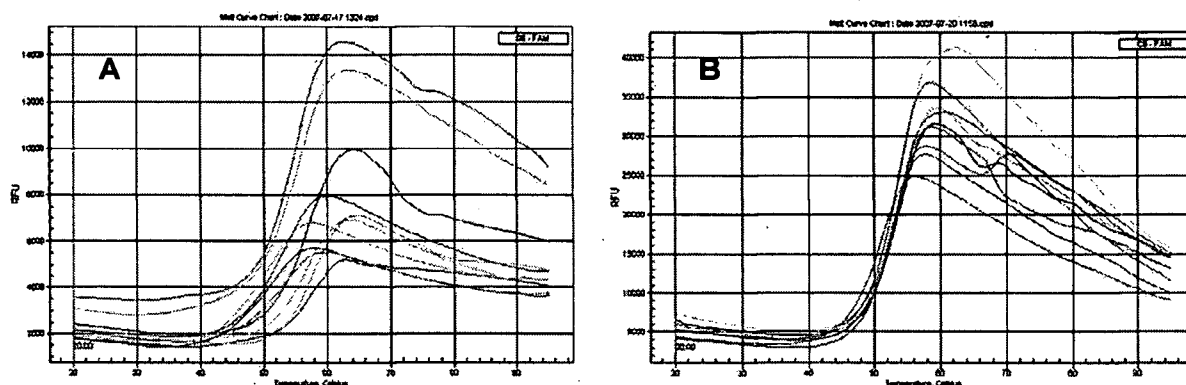


Figure 26: examples of Thermofluor data from PTB2 (A) and PTB2-MBP (B)

X-axis...Temperature [°C]; Y-axis...RFU (fluorescence emission intensity);

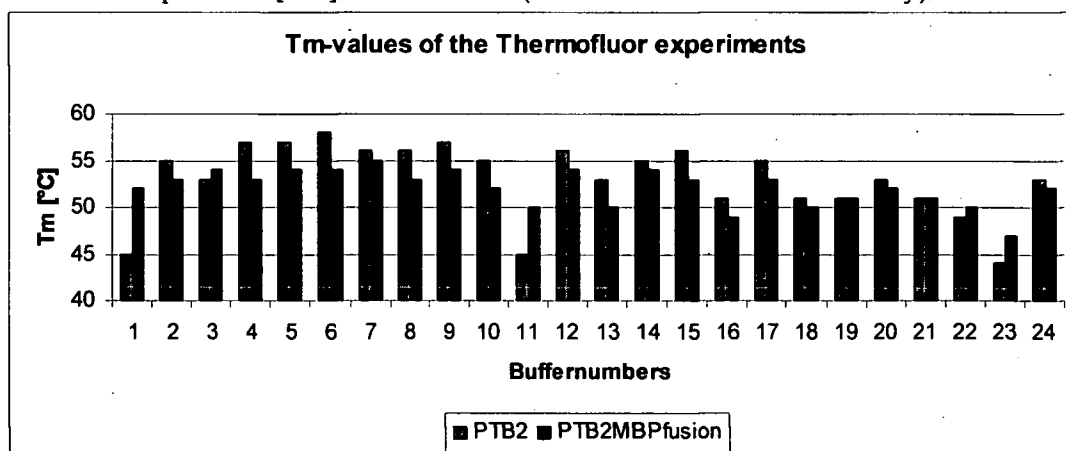


Figure 27: Summary of thermofluor results

The buffers with the highest melting temperatures for the soluble protein are the best stabilizing condition. The buffer conditions are listed in the Appendix. Buffer 4 to Buffer 7 seemed to be the best buffers both for PTB2

and for the fusion protein. Even though the results are similar it can be clearly seen in Figure 26 that MBP stabilizes the protein to a certain amount. Buffers 4-6 of the mentioned buffers are phosphate buffers in the pH range from 5 to 6. Twenty and 22 which are similar buffers as the Tris buffer before optimization and they did not seem to stabilize the protein construct as well as the phosphate buffers.

Solubility cleavage screen:

In the cleavage screen the Tris buffer seemed to solubilize the protein enough during the release of the MBP tag. However, the phosphate buffer pH 7 had the same amount of protein in solution after cleavage although there was no salt, detergent or APP peptide added as in the Tris conditions respectively (data not shown). This suggests that the phosphate buffer itself is stabilizing the protein already much more than the Tris buffer.

IBS Solubility Kit (Jena Bioscience):

Most of the buffers tested in the Solubility Kit showed protein aggregation after over night incubation at 18°C. The drops without aggregation were diluted to 50µL in the same buffers and then measured in the DLS spectrometer. None of the conditions showed monodispersity. The fact that all of the conditions lead to aggregation, showed again how unstable this protein is. Especially the overnight incubation at 18°C and the high sensitivity of the DLS technique for even small aggregations lead to this disappointing result.

Conclusion from the Buffer screens:

The general conclusion from the buffer screen is that a phosphate buffer is more favorable for the stability and solubility of this protein. However, the pH values differed strongly between the screens ranging from pH 5.5 - 8. The phosphate buffer at pH 5.5 and 6 was tested in the purification protocol and showed aggregation of the protein right after the lysis. Therefore the next test was to try the phosphate buffer with pH 7. The results from using this buffer are shown in the next section.

3.2.5 Optimized Purification

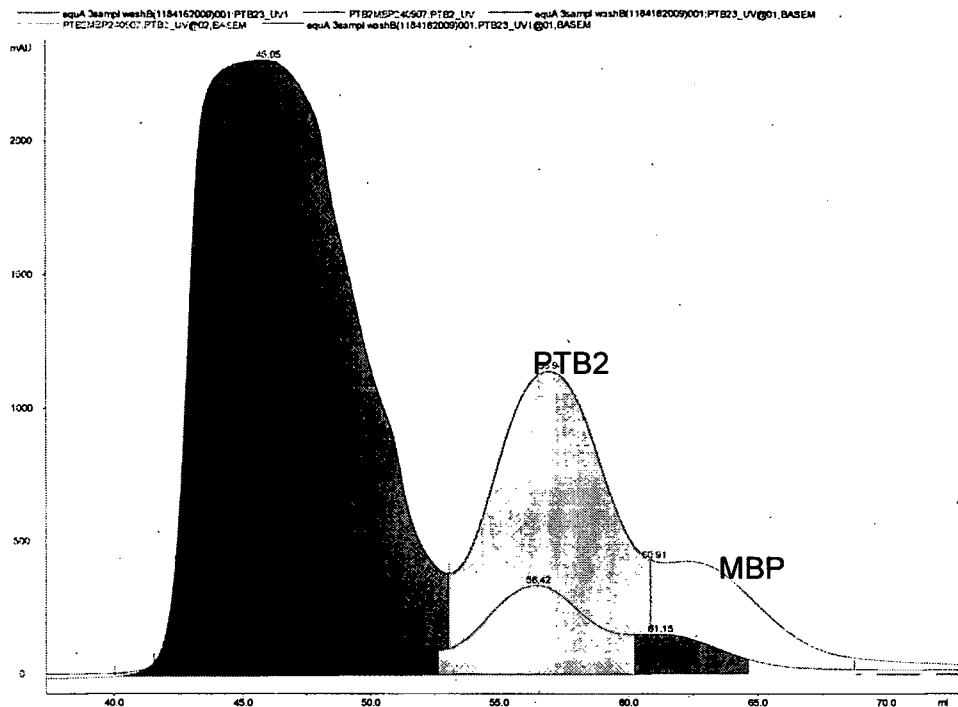


Figure 28: Chromatogram-overlay of a superdex-75 size exclusion chromatography of PTB2.

5mL of the PTB2-MBP fusion protein were separated from aggregation over a superdex-75 gel filtration column. The chromatogram in the front of Figure 28 shows the protein purified in Tris-buffer (pH 8). The chromatogram in the back shows the protein purified in phosphate buffer (pH 7). The purifications were performed in an identical way using the same amount of cells, lysate and elution. The ratio of 1/6 soluble protein to aggregates changes to 1/3 in the phosphate buffer pH 7, this indicates an increase by one third in solubility after the buffer change.

In the Figure 29 the last purification step of PTB2 is shown. The chromatogram on the one hand highlights the high amount of aggregation after cleavage of the purification tag MBP. However, on the other hand the high concentrations of protein show the success of the optimization effort and explain the higher ratio of aggregates to solutes.

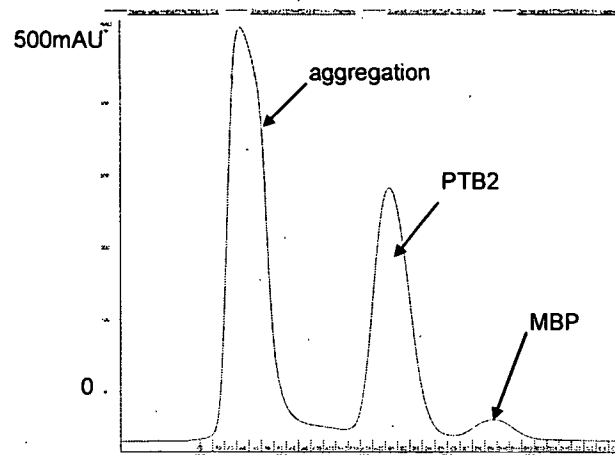


Figure 29: Second size exclusion chromatography step for PTB2

The purification was optimized for the PTB2 construct, since it represents the main focus in the characterization of this domain. However, the similar characteristics of the PTB1+2 construct lead to the decision to purify this construct under the same optimized buffer conditions. In Figure 30 the success of this purification can be seen

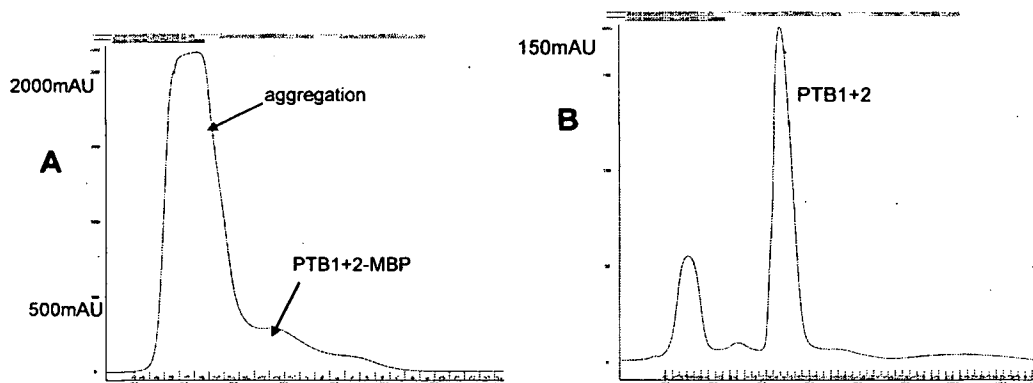


Figure 30: FPLC-Chromatograms of PTB1+2 of the first (A) and the second (B) size exclusion chromatography steps.

The chromatograms from Fig 29, 30 were collected from a superdex 75 column with 120mL total volume and 5mL sample volume. The vast amount of aggregation is depicted in chromatogram 30A, which shows the direct separation of the elution from the affinity beads. In chromatogram 30B, after cleavage of the MBP tag some protein is aggregated but the majority remains stable.

3.2.6 Protein Analysis

To analyze the quality of the obtained PTB2 domain the following methods were applied. At first DLS measurements were performed to determine the amount of polydispersity in the sample.

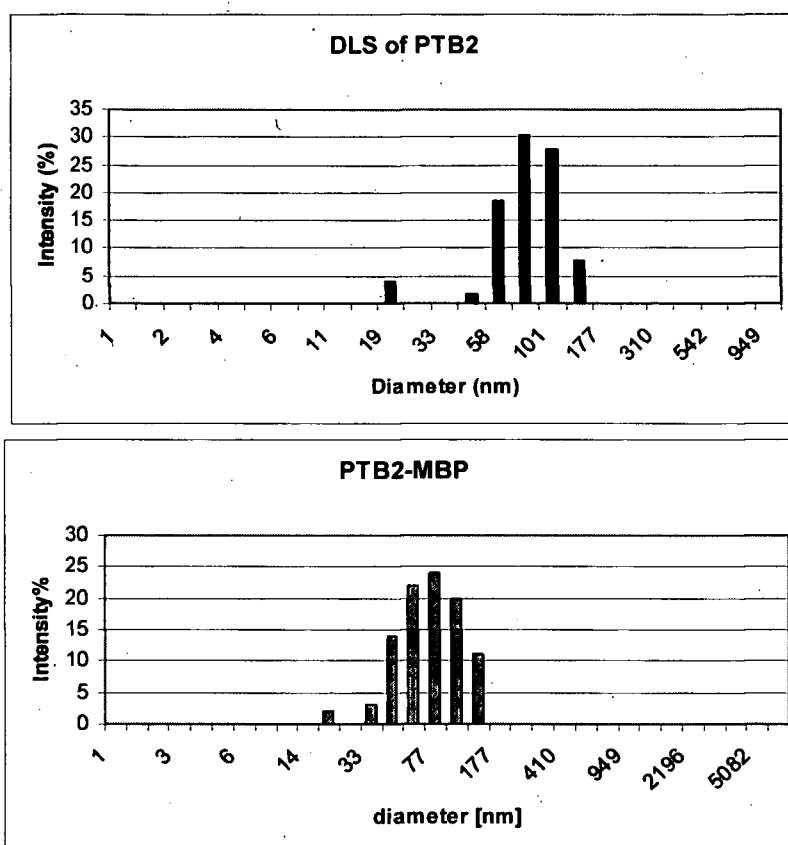


Figure 31: DLS measurement of PTB2 (purple) and PTB2-MBP fusion protein (blue).

An ideal monodisperse solution has one peak with 100% intensity. The DLS results show polydispersity even after buffer optimization. Also, the mean diameter of the protein should be smaller (PTB2 approx 5nm; MBP-PTB2 approx 15nm). The fusion protein therefore may be less aggregated since the diameter is of about the same size in both measurements. DLS is not reliable for unstable proteins, since it is sensitive to aggregation. Some small aggregates can hinder the measurement of the soluble protein.

As a second approach CD spectroscopy was applied to check whether the PTB2 domain is properly folded. Figure 32 shows a published CD spectrum of Fe65. This spectrum was used as a comparison for our CD data.

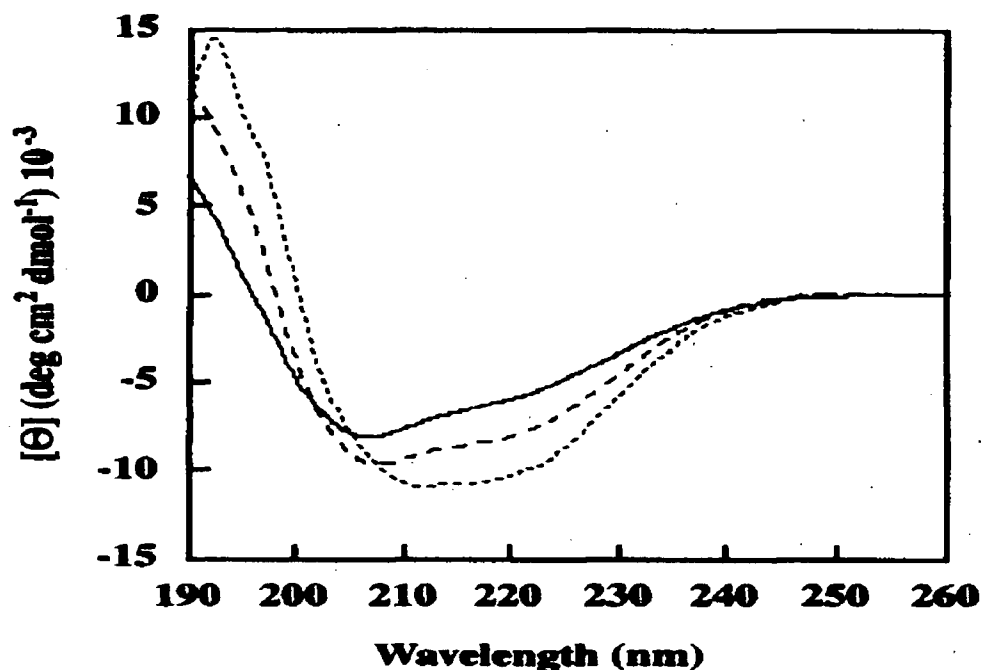


Figure 32: CD spectra of Fe65.⁴⁹

His-tagged Fe65, PTB2 and PTB1+2 were measured at 25°C in 10mM phosphate buffer pH10. continuous line...Fe65, dashed line...PTB1+2, dotted line...PTB2.

With the following equation the ellipticity was calculated from the raw data:

$$\Theta = (\text{mdeg} \times 100) / N \times l \times c$$

(N= number of amino acid residues; l= path length [cm]; c= concentration [mM])

⁴⁹ Cf. Lamberti A et al, 2005, Biosci Biotechnol Biochem., 12: p.2397-2398

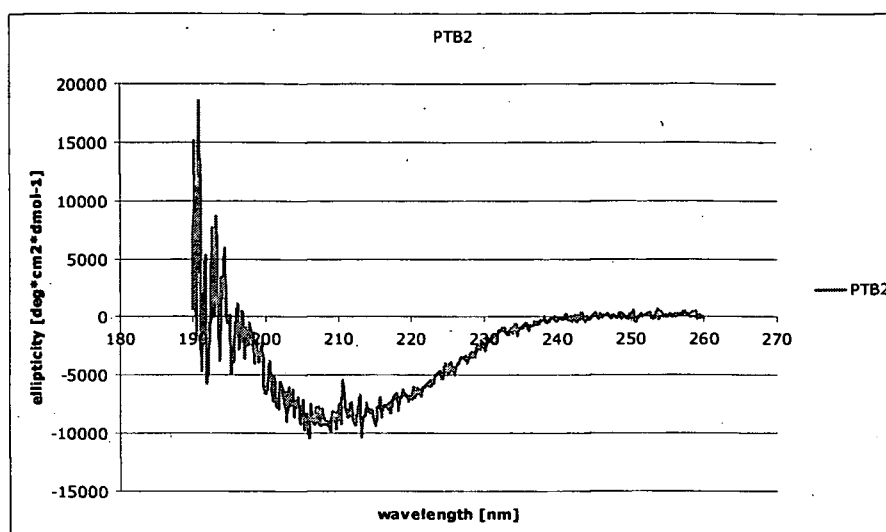


Figure 33: CD spectrum of the PTB2 domain.

5 μ M solution of Fe65 PTB2 domain was measured at 20°C in 20mM phosphate buffer.

Compared to the previously published spectrum in Figure 32 the PTB2 domain looks well organized, since the peaks at 220 and 200nm are very similar in both spectra. Even with the low concentration of the PTB2 domain (around 5 μ M) enough signals were obtained to show that the domain is folded.

3.2.7 ITC with AICD

In the ITC binding studies the binding strength of the PTB2 domain to the AICD peptide was determined. The chosen peptide of the APP intracellular domain contains the known PTB binding motif NPXY.

The following peptides were used in the ITC experiments.

mAPP: DAAVTPEERHLSKMQQNGYEAPTAKFFEQ

APP: DAAVTPEERHLSKMQQNGYENPTYKFFEQ

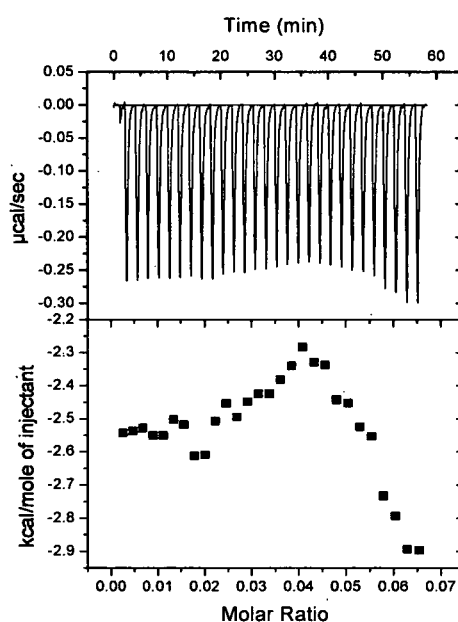


Figure 34: ITC measurement of buffer blank with APP peptide

Example of a buffer blank run with 25 μ M AICD peptide; 10 μ L per injection.

Figure 34 shows the negative control, in which no binding can be seen, since no protein is around. This buffer blank was subtracted from all the measurements with the APP peptide to show that the injection of the peptide alone is not significant heat release.

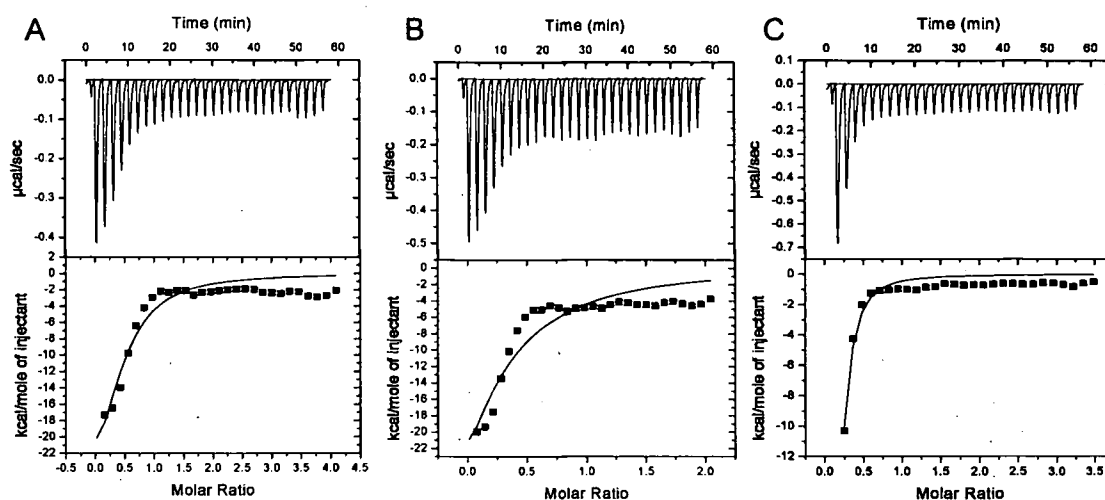


Figure 35: ITC measurement of PTB2 with APP peptide

(10 μ L per injection)

A: 4 μ M PTB2 domain binding to 25 μ M AICD peptide, ratio PTB2:AICD = 1:7.

B: 8 μ M PTB2 domain binding to 25 μ M AICD peptide, ratio PTB2:AICD = 1:4.

C: 4 μ M PTB2 domain binding to 50 μ M AICD peptide, ratio PTB2:AICD = 1:12.5.

The fast saturation of the PTB2 domain with the APP peptide is clearly indicated in Figure 35 by the small number of injections that are needed to reach saturation. To achieve a more sigmoidal shaped curve the peptide amount has to be reduced slightly in the protein to peptide ratio. In this case it is also most important to increase the protein concentration, since then a stronger and more accurate signal can be obtained.

In Fig 35B the protein was more concentrated and still the curve is not ideally shaped and the signal is not increased. This is most probably due to the concentrating of the protein sample before this measurement. Concentrating usually caused the protein to aggregate, therefore it could be aggregated during the measurement, and the concentration of functional protein may be much lower. The optimum ratio was achieved in Figure 35A, where the curve is already slightly sigmoidal shaped. The mean value of the dissociation constant from 4 measurements is $3\mu\text{M}\pm 0.6$.

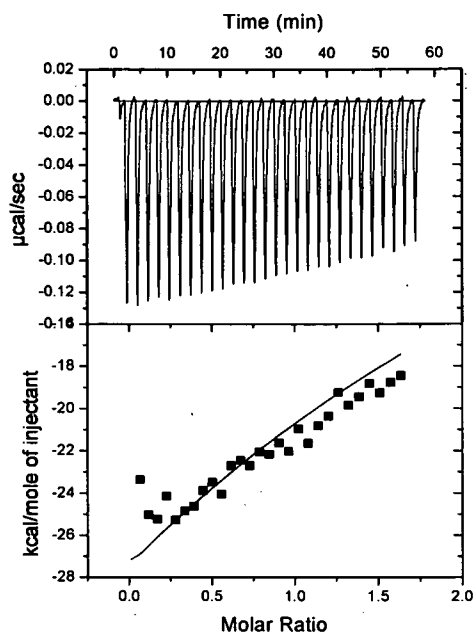


Figure 36: ITC measurement of mutated APP peptide and PTB2 domain.

4 μM PTB2 domain with 150 μM mAICD peptide, ratio PTB2-MBP:AICD = 1:37.5; 10 μL injection.

In Figure 36 very little binding can be seen, which is most probably due to the background reaction heat of two different solutes meeting each other. This measurement is the evidence that the PTB2 domain is binding to exactly the binding motif on the APP peptide that was mutated in this peptide.

Conclusion and Future Perspectives

From the experiments that were performed in the context of this project, the first question of whether the WW domain is binding to other parts of Fe65 could not be answered clearly. Neither in the Pull-Down assays nor in the ITC measurements was binding detected. However, the purification of the PTB2 domain could be optimized to reach a reasonable yield of protein for further experiments. The domain was well-folded, but was polydisperse in solution. After the ITC experiments it was clear that the PTB2 domain is folded natively, otherwise binding to its ligand, the APP intracellular domain would not occur. Apart from the dissociation constant for the Interaction of Fe65 to APP another phenomenon could be determined. The ITC experiments showed that the MBP tagged PTB2 domain is not able to bind to its ligands. This fact is not only interesting for further experiments with the PTB2 domain, but also explains why the WW domain was not able to bind to the MBP tagged PTB domain constructs, in the Pull-Down assays.

In order to check the hypothesis of Cao et al the constructs could be labeled in a different way for GST Pull-Downs with the WW domain. Smaller tags that may interfere less could help to make the constructs accessible for WW domain binding. In case this model could be proven, another future aspect would be to try getting a snapshot of this binding in the form of a crystal structure. Furthermore, the optimization of the purification protocol for PTB2 is still not perfect, since much protein is lost due to aggregation. Therefore optimization would still be another important future plan to get more soluble protein for structural studies. One of the most important future approaches towards understanding the interaction to APP would be solving the crystal structure of the PTB2 domain bound to AICD.

Another interesting fact is that the c-Abl tyrosine kinase is phosphorylating Tyr547 within the PTB2 domain and thereby enhancing transcriptional

transactivation.⁵⁰ At the same time it is known to be bound by the WW domain. These findings suggest that the WW domain could recruit the kinase to facilitate the interaction with the PTB2 domain. It was also reported that the WW domain is binding to the PTB2 domain *in vitro*⁵¹ and thereby may prevent binding of the c- Abl kinase. If this is true *in vivo* as well, then binding of the c-Abl kinase and other ligands to the WW domain could open up the “inactive” protein. Then c-Abl could phosphorylate the PTB2 domain, which is known to stimulate Fe65/APP mediated gene transcription.⁵² Due to this process the accessibility of PTB2 for AICD could be increased, which could activate transcription.

To check whether the c-Abl tyrosine kinase is actually the missing part in Cao et al’s model, which activates (opens) the Fe65 adaptor protein would be another interesting future approach. First of all co-localization of PTB2 and c-Abl *in vivo* has to be shown and later on *in vitro* testing like *in vitro* phosphorylation is important to check these findings.

Since there is only controversial data about possible target genes that are regulated by Fe65 an important future experiment would be also to look more carefully for the promoters that the Fe65 gene activating complex is binding to. A CHIP on chip experiment would be a reliable high-throughput method to address this question. Maybe after unveiling some of the mysteries of the intracellular signaling cascade of APP the question of the physiological role of APP could be answered more clearly. In the end it would perhaps help to find the trigger of Alzheimer’s disease in this maze of interacting proteins.

⁵⁰ Cf. Standen CL et al, 2003, *Mol Cell Neurosci*, **24**: 851-857.

⁵¹ Cf. Cao X et al, 2004, *J Biol Chem* **279**: 24601-24611.

⁵² Cf. Perkington et al, 2004, *J Biol Chem* **279**: 22084-22091.

Bibliography

- Baek SH, Ohgi KA, Rose DW, Koo EH, Glass CK, Rosenfeld MG. 2002. Exchange of N-CoR corepressor and Tip60 coactivator complexes links gene expression by NF- κ B and -amyloid precursor protein. *Cell* **110**: 55-67.
- Bressler SL, Gray MD, Sopher BL, Hu QB, Hearn MG, Pham DG, Dinulos MB, Fukuchi KI, Sisodia SS, Miller MA, Distèche CM, Martin GM. 1996. cDNA cloning and chromosome mapping of the human Fe65 gene: interaction of the conserved cytoplasmic domains of the human -amyloid precursor protein and its homologues with the mouse Fe65 protein. *Hum Mol Genet* **5**: 1589-1598.
- Bruni P, Minopoli G, Brancaccio T, Napolitano M, Faraonio R, Zambrano N, Hansen U, Russo T. 2002. Fe65, a ligand of the Alzheimer's -amyloid precursor protein, blocks cell cycle progression by down-regulating thymidylate synthase expression. *J Biol Chem* **277**: 35481-35488.
- Cao X, Sudhof TC. 2001. A transcriptionally [correction of transcriptively] active complex of APP with Fe65 and histone acetyltransferase Tip60. *Science* **293**: 115-120.
- Cao X, Sudhof TC. 2004. Dissection of amyloid- precursor protein-dependent transcriptional transactivation. *J Biol Chem* **279**: 24601-24611.
- Chang KA, Kim HS, Ha TY, Ha JW, Shin KY, Jeong YH, Lee JP, Park CH, Kim S, Baik TK, Suh YH. 2006. Phosphorylation of amyloid precursor protein (APP) at Thr668 regulates the nuclear translocation of the APP intracellular domain and induces neurodegeneration. *Mol Cell Biol* **26**: 4327-4338.
- Ermekova KS, Zambrano N, Linn H, Minopoli G, Gertler F, Russo T, Sudol M. 1997. The WW domain of neural protein FE65 interacts with proline-rich motifs in Mena, the mammalian homolog of Drosophila enabled. *J Biol Chem* **272**: 32869-32877.
- Esposito F, Ammendola R, Duilio A, Costanzo F, Giordano M, Zambrano N, Dagostino P, Russo T, Cimino F. 1990. Isolation of cDNA fragments hybridizing to rat brain-specific mRNAs. *Dev Neurosci* **12**: 373-381.
- Farooq A, Zhou MM, 2004; PTB or not to be: promiscuous, tolerant and Bizarro domains come of age. *IUBMB Life*; **56**(9):547-57.

- Gralle M, Ferreira ST., 2007, Structure and functions of the human amyloid precursor protein: the whole is more than the sum of its parts. *Prog Neurobiol*; 82(1):11-32.
- Harding SE, Jumel K, 1998, Unit 7.8 in: *Current protocols in protein science*, John Wiley publishers.
- Kasper DL, Braunwald E, Fauci AS, Hauser SL, Longo DL, Jameson JL, eds. *Harrison's Principles of Internal Medicine*. 16th ed. New York: McGraw-Hill, 2005:1505-1508.
- Kim HS, Kim EM, Lee JP, Park CH, Kim S, Seo JH, Chang KA, Yu E, Jeong SJ, Chong YH, Suh YH. 2003. C-terminal fragments of amyloid precursor protein exert neurotoxicity by inducing glycogen synthase kinase-3 expression. *FASEB J* 17: U253-U280.
- EK Koepf, HM Petrassi, M Sudol and JW Kelly; 1999; WW: An isolated three-stranded antiparallel beta-sheet domain that unfolds and refolds reversibly; evidence for a structured hydrophobic cluster in urea and GdnHCl and a disordered thermal unfolded state; *Protein Sci* 8: 841-853
- Laemmli, 1970, Cleavage of structural proteins during the assembly of the head of bacteriophage T4. *Nature*: 15; 227(5259):680-5.
- Lamberti A, Longo O, Del Vecchio P, Zambrano N, Barone G, Russo T, Arcari P., 2005, Probing the secondary structure of a recombinant neuronal adaptor protein and its phosphotyrosine binding domains; *Biosci Biotechnol Biochem.*;69(12):2395-400.
- Lambrechts A, Kwiatkowski AV, Lanier LM, Bear JE, Vandekerckhove J, Ampe C, Gertler FB. 2000. cAMP-dependent protein kinase phosphorylation of EVL, a mena/VASP relative, regulates its interaction with actin and SH3 domains. *J Biol Chem* 275: 36143-36151.
- Lovestone S, Reynolds CH, Latimer D, Davis DR, Anderton BH, Gallo JM, Hanger D, Mulot S, Marquardt B, Stabel S, Woodgett JR, Miller CCJ. 1994. Alzheimer's disease-like phosphorylation of the microtubule-associated protein tau by glycogen synthase kinase-3 in transfected mammalian cells. *Curr Biol* 4: 1077-1086.
- McLoughlin DM, Miller CCJ; 2007; The Fe65 proteins and Alzheimer's disease; *J Neurosci Res*, [ahead of print].
- Meiyappan M, Birrane G, Ladas JA. 2007; Structural basis for polyproline recognition by the FE65 WW domain. *J Mol Biol.* 28; 372(4):970-80. Epub 2007 Jun 29.

- Pain R, 2004, Unit 7.6 in: Current protocols in protein science. John Wiley publishers.
- Pardossi-Piquard R, Petit A, Kawarai T, Sunyach C, da Costa CA, Vincent B, Ring S, D'Adamio L, Shen J, Muller U, Hyslop PS, Checler F. 2005. Presenilin-dependent transcriptional control of the A - degrading enzyme neprilysin by intracellular domains of beta APP and APLP. *Neuron* 46: 541-554.
- Perkinton MS, Standen CL, Lau KF, Kesavapany S, Byers HL, Ward M, McLoughlin DM, Miller CCJ. 2004. The c-Abl tyrosine kinase phosphorylates the Fe65 adaptor protein to stimulate Fe65/amyloid precursor protein nuclear signaling. *J Biol Chem* 279: 22084-22091.
- Sabo SL, Ikin AF, Buxbaum JD, Greengard P. 2003. The amyloid precursor protein and its regulatory protein, FE65, in growth cones and synapses in vitro and in vivo. *J Neurosci* 23: 5407-5415.
- Sambrook J, 2001, *Molecular Cloning: A Laboratory Manual*, 3rd edition
- Standen CL, Perkinton MS, Byers HL, Kesavapany S, Lau KF, Ward M, McLoughlin D, Miller CCJ. 2003. The neuronal adaptor protein Fe65 is phosphorylated by mitogen-activated protein kinase (ERK1/2). *Mol Cell Neurosci* 24: 851-857.
- Sudol M, Sliwa K, Russo T. 2001. Functions of WW domains in the nucleus. *FEBS Lett* 490: 190-195.
- Telese F, Bruni P, Donizetti A, Gianni D, D'Ambrosio C, Scaloni A, Zambrano N, Rosenfeld MG, Russo T. 2005. Transcription regulation by the adaptor protein Fe65 and the nucleosome assembly factor SET. *EMBO Rep* 6: 77-82.
- Uhlik MT, Temple B, Bencharit S, Kimple AJ, Siderovski DP, Johnson GL. 2005. Structural and evolutionary division of phosphotyrosine binding (PTB) domains. *J Mol Biol.* 7; 345(1):1-20.
- Vardy ERLC, Catto AJ, Hooper NM. 2005. Proteolytic mechanisms in amyloid- metabolism: therapeutic implications for Alzheimer's disease. *Trends Mol Med* 11: 464-472.
- von Rotz RC, Kohli BM, Bosset J, Meier M, Suzuki T, Nitsch RM, Konietzko U. 2004. The APP intracellular domain forms nuclear multiprotein complexes and regulates the transcription of its own precursor. *J Cell Sci* 117: 4435-4448.

- Walsh DM, Selkoe DJ. 2004. Deciphering the molecular basis of memory failure in Alzheimer's disease. *Neuron* 44: 181-193.
- World Health Organization. 2000. *The World Health Report 2000 - health systems: improving performance*. Geneva: World Health Organization.
- Zambrano N, Minopoli G, De Candia P, Russo T. 1998. The Fe65 adaptor protein interacts through its PID1 domain with the transcription factor CP2/LSF/LBP1. *J Biol Chem* 273: 20128-20133.
- Zhang Z, Lee CH, Mandiyan V, Borg JP, Margolis B, Schlessinger J, Kuriyan J. 1997; Sequence-specific recognition of the internalization motif of the Alzheimer's amyloid precursor protein by the X11 PTB domain. *EMBO J.* 15; 16(20):6141-50.

Internet Sources

- URL: http://www.alz.org/alzheimers_disease_what_is_alzheimers.asp
- URL: <http://www.crystalinks.com/alzheimers.html>.
- URL: http://www.alz.org/alzheimers_disease_what_is_alzheimers.asp.
- URL: <http://www.ncbi.nlm.nih.gov/entrez/viewer.fcgi?db=protein&id=4502131>.
- URL: <http://www.ebi.ac.uk/Tools/clustalw2/index.html>.
- URL: <http://www.ncbi.nlm.nih.gov/blast/BLAST/blastp/Formatting>.
- URL: <http://bioinf.cs.ucl.ac.uk/psipred/psiform.html>.
- URL: <http://www.fermentas.com/catalog/electrophoresis/proteinstaining>.
- URL: <http://www.expasy.ch/tools/protparam>.
- URL: <http://www.rcsb.org/pdb/home/home.do>

Appendix

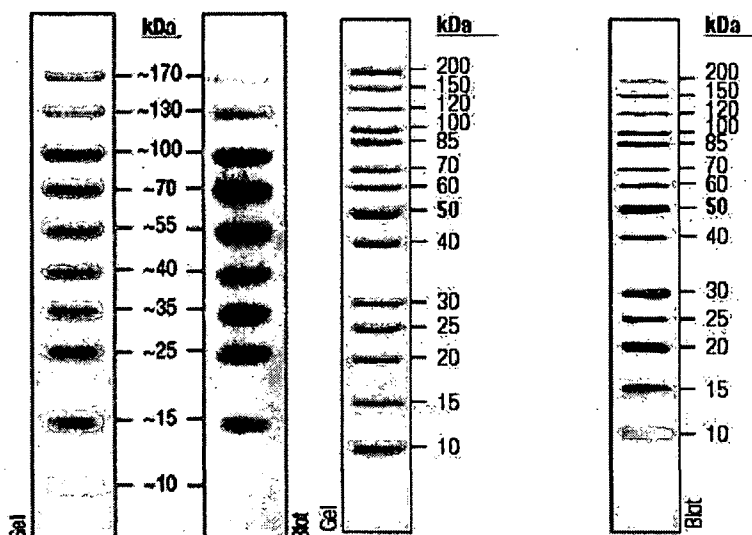


Figure 37: pre-stained (left) and unstained (right) Page Ruler from Fermentas

	1	2	3	4	5	6
A	Sodium acetate pH 4.5	Sodium citrate pH 4.7	Sodium acetate pH 5	Potassium phosphate pH 5	Sodium phosphate pH 5.5	Sodium citrate pH 5.5
B	Sodium acetate pH 4.5	Sodium citrate pH 4.7	Sodium acetate pH 5	Potassium phosphate pH 5	Sodium phosphate pH 5.5	Sodium citrate pH 5.5
C	Sodium acetate pH 4.5	Sodium citrate pH 4.7	Sodium acetate pH 5	Potassium phosphate pH 5	Sodium phosphate pH 5.5	Sodium citrate pH 5.5
D	Sodium acetate pH 4.5	Sodium citrate pH 4.7	Sodium acetate pH 5	Potassium phosphate pH 5	Sodium phosphate pH 5.5	Sodium citrate pH 5.5
E	Potassium phosphate pH 7	Hepes pH 7	Ammonium acetate pH 7.3	Sodium phosphate pH 7.5	Tris pH 7.5	Imidazole pH 8
F	Potassium phosphate pH 7	Hepes pH 7	Ammonium acetate pH 7.3	Sodium phosphate pH 7.5	Tris pH 7.5	Imidazole pH 8
G	Potassium phosphate pH 7	Hepes pH 7	Ammonium acetate pH 7.3	Sodium phosphate pH 7.5	Tris pH 7.5	Imidazole pH 8
H	Potassium phosphate pH 7	Hepes pH 7	Ammonium acetate pH 7.3	Sodium phosphate pH 7.5	Tris pH 7.5	Imidazole pH 8
	7	8	9	10	11	12
A	Mes pH 5.8	Potassium phosphate	Mes pH 6.2	Sodium phosphate	Sodium cacodylate	Mes pH 6.5

		pH 6		pH 6.5	pH 6.5	
B	Mes pH 5.8	Potassium phosphate pH 6	Mes pH 6.2	Sodium phosphate pH 6.5	Sodium cacodylate pH 6.5	Mes pH 6.5
C	Mes pH 5.8	Potassium phosphate pH 6	Mes pH 6.2	Sodium phosphate pH 6.5	Sodium cacodylate pH 6.5	Mes pH 6.5
D	Mes pH 5.8	Potassium phosphate pH 6	Mes pH 6.2	Sodium phosphate pH 6.5	Sodium cacodylate pH 6.5	Mes pH 6.5
E	Hepes pH 8	Tris pH 8	Bicine pH 8	Tris pH 8.5	Bicine pH 9	water
F	Hepes pH 8	Tris pH 8	Bicine pH 8	Tris pH 8.5	Bicine pH 9	water
G	Hepes pH 8	Tris pH 8	Bicine pH 8	Tris pH 8.5	Bicine pH 9	water
H	Hepes pH 8	Tris pH 8	Bicine pH 8	Tris pH 8.5	Bicine pH 9	water

Table 7: 96 Thermoflour buffer conditions